The COBE DIRBE Point Source Catalog

Beverly J. Smith

Department of Physics, Astronomy, and Geology, East Tennessee State University, Box 70652, Johnson City, TN 37614

smithbj@etsu.edu

Stephan D. Price

Air Force Research Laboratory, Space Vehicles Directorate, 29 Randolph Road, Hanscom AFB, MA 01731

Steve.Price@hanscom.af.mil

Rachel I. Baker

Department of Physics and Astronomy, East Tennessee State University, Box 70652, Johnson City, TN 37614

zrih1@yahoo.edu

Received _______________________; accepted _______________________

ABSTRACT

We present the COBE DIRBE Point Source Catalog, an all-sky catalog containing infrared photometry in 10 infrared bands from 1.25 μm and 240 μm for 11,788 of the brightest near and mid-infrared point sources in the sky. Since DIRBE had excellent temporal coverage ($100 - 1900$ independent measurements per object during the 10 month cryogenic mission), the Catalog also contains information about variability at each wavelength, including amplitudes of variation observed during the mission. Since the DIRBE spatial resolution is relatively poor ($0.7°$), we have carefully investigated the question of confusion, and have flagged sources with infrared-bright companions within the DIRBE beam. In addition, we filtered the DIRBE light curves for data points affected by companions outside of the main DIRBE beam but within the 'sky' portion of the scan. At high Galactic latitudes ($|b| > 5°$), the Catalog contains essentially all of the unconfused sources with flux densities greater than 90, 60, 60, 50, 90, and 165 Jy at 1.25, 2.2, 3.5, 4.9, 12, and 25 μm, respectively, corresponding to magnitude limits of approximately 3.1, 2.6, 1.7, 1.3, -1.3, and -3.5. At longer wavelengths and in the Galactic Plane, the completeness is less certain because of the large DIRBE beam and possible contributions from extended emission. The Catalog also contains the names of the sources in other catalogs, their spectral types, variability types, and whether or not the sources are known OH/IR stars. We discuss a few remarkable objects in the Catalog, including the extremely red object OH 231.8+4.2 (QX Pup), an asymptotic giant branch star in transition to a proto-planetary nebula, which has a DIRBE 25 μm amplitude of 0.29 ± 0.07 magnitudes.

Subject headings: stars: AGB and post-AGB, stars: variable: Miras, astronomical databases: catalogs, infrared: stars

1. Introduction

Infrared surveys provide a window on the content and structure of the Galaxy, being relatively free of the interstellar extinction that compromises measurements at shorter wavelengths. Since the nature of the brightest sources in the sky changes with the infrared wavelength and the majority of these objects are variable, measurements over a large wavelength baseline with a fairly dense sampling in time are needed to fully characterize the sources. At optical and near-infrared wavelengths ($\leq$3 μm), the spectral energy distributions of stars are dominated by radiation from the stellar photosphere, while in the mid-infrared ($\geq$6 μm), emission from circumstellar dust becomes important. In the near-infrared (0.9 $-$ 2.2 μm), the sky was first surveyed by the Two Micron Sky Survey (TMSS; Neugebauer & Leighton (1969)), and more recently by the Two Micron All Sky Survey (2MASS; Cutri et al. (2003)) and the DENIS survey (Epchtein et al. 1999). The Infrared Astronomical Satellite (IRAS) survey covered almost the whole sky in the 12 $-$ 100 μm spectral range (Beichman et al. 1988). The small gaps in the IRAS mid-infrared coverage have since been filled in by the Midcourse Space Experiment (MSX) mission (Price et al. 1999). The most complete survey made so far in the intermediate spectral region between 3 and 6 μm was the Air Force Geophysical Laboratory (AFGL) Infrared Sky Survey, which covered 71% of the sky to a sensitivity of 90 Jy at 4.2 μm (Price & Walker 1976). The more sensitive MSX survey (Price et al. 1999) covered only $\sim$15% of the sky (two-thirds of which was within 6° of the Galactic Plane) to a point source limit at 4.3 μm of $\sim$20 Jy.

There is another untapped infrared database suitable for the construction of an infrared point source catalog: the archival data from the Diffuse Infrared Background Experiment (DIRBE) (Hauser et al. 1998) on the Cosmic Background Explorer (COBE) satellite (Boggess et al. 1992). DIRBE operated at cryogenic temperatures for 10 months in 1989-1990, providing full-sky coverage at 10 infrared wavelengths (1.25, 2.2, 3.5, 4.9, 12, 25, 60, 100, 140, and 240 μm). Although DIRBE was designed to search for the cosmic infrared background, the data are also useful for studying point sources, in spite of its relatively poor spatial resolution (0.7°). To date, however, point source fluxes from DIRBE have been little utilized. During the mission, DIRBE stellar fluxes were mainly used for calibration verification (Burdick & Murdock 1997; Cohen 1998). Recently, we used the DIRBE database to extract high quality $1.25 - 25$ μm time-sequence infrared photometry for 38 known Mira variable stars (Smith et al. 2002) and 207 high Galactic latitude 12 μm-selected sources (Smith 2003), while Knapp et al. (2003) extracted DIRBE 2.2 μm light curves for a few dozen known variable stars. These studies showed that DIRBE provided good stellar photometry in the six shortest wavelengths. At 4.9 μm, the sensitivity per measurement is $\sim$10 Jy (Smith et al. 2002), about a magnitude fainter than the AFGL survey. Thus DIRBE covers the 85% of the sky not surveyed by MSX to a sensitivity per scan at $\sim$4 μm similar to that of MSX.

Another DIRBE advantage is its excellent temporal coverage, that permits a careful investigation of possible infrared variability of stars. A typical location on the sky was observed $10 - 15$ times during the course of a week, and, on the average, about 200 times during the 10 month cryogenic mission (Hauser et al. 1998). The DIRBE coverage varied with position on the sky. Sources near the ecliptic poles were observed approximately twice a day, producing $400 - 1000$ observations over the mission. Near the ecliptic plane, sources were typically observed roughly twice a day for 2 months, then were inaccessible for 4 months before coming back into view. By comparison, IRAS typically provided only two or three independent flux measurements of a star at 12 μm (Little-Marenin & Stencel 1992), while MSX made up to six observations over a four month period (Egan et al. 1999).

In this paper, we describe the DIRBE Point Source Catalog, a database of infrared photometry and variability information for the brightest sources in the infrared sky. In the Smith et al. (2002) study, we specifically targeted asymptotic giant branch (AGB) stars that were known to be Mira variables. Consequently, we neglected non-Mira AGB stars, infrared-bright non-AGB stars, Miras not previously classified as Miras, and very dust-enshrouded stars without bright optical counterparts. In Smith (2003), we studied a complete 12 μm flux-limited sample of 207 IRAS sources at Galactic latitudes $|b| > 5°$. This study neglected bright stars at the shorter DIRBE wavelengths or at 25 μm, as well as stars in the Galactic plane. In the current study, we constructed an all-sky DIRBE Point Source Catalog that extends these earlier studies to include all sources above a uniform signal to noise selection criterion in each of the six shortest wavelength DIRBE bands, as well as sources in the Galactic Plane. The present Catalog contains essentially all of the unconfused high Galactic latitude point sources detected by DIRBE in the six shorter wavelength filters with S/N per individual scan greater than $3 - 9$. These levels are sufficient to provide good light curves. In the Galactic plane and at longer wavelengths the Catalog is less complete.

2. Sample Selection

Unlike the IRAS and 2MASS Catalogs, the DIRBE Point Source Catalog was not constructed by searching the DIRBE database with a point source template and extracting sources based on signal to noise and confirmation criteria. The DIRBE Catalog was constructed using a target sample list obtained from other infrared catalogs. Since DIRBE is much less sensitive per scan than IRAS or 2MASS, essentially all of the point sources with high S/N light curves in the DIRBE database are already contained in IRAS, 2MASS, and/or MSX. Thus for simplicity we used these previous catalogs to select a sample for the DIRBE Point Source Catalog.

Our initial sample included a total of 21,335 sources; the final Catalog contains 11,788 sources. The initial sample was selected from the IRAS Point Source Catalog (1988), the 2MASS Point Source Catalog (Cutri et al. 2003), and/or the MSX Point Source Catalog Version 1.2 (Egan et al. 1999) that satisfied at least one of the following criteria: a) 2MASS J magnitude ≤ 4.51 ($F_{1.25} \geq 25$ Jy), b) 2MASS K magnitude ≤ 3.81 ($F_{2.2} \geq 20$ Jy), c) IRAS or MSX $F_{12} \geq 15$ Jy, or d) IRAS or MSX $F_{25} \geq 27.5$ Jy. The 1.25 and 2.2 μm limits are equal to the average 1σ sensitivity per scan in the raw DIRBE light curves of Smith et al. (2002), while the 12 and 25 μm limits are 0.5 $\times$ the average noise levels per scan in that study. These low limits were selected in order to avoid missing variable stars that may have been faint during the 2MASS, IRAS, or MSX mission, and to improve the completeness at 3.5 and 4.9 μm (see Section 6). Since the filtering process improves the average per-measurement uncertainty (see Section 5), a sensitive selection criterion is warranted to include as many sources as possible.

There are 7,872 sources with 2MASS J ≤ 4.51, 20,492 sources with 2MASS K ≤ 3.81, 4,969 sources with IRAS $F_{12} \geq 15$ Jy, 40 sources in the MSX IRAS Gaps survey with MSX $F_{12} \geq 15$ Jy, 2,753 sources with IRAS $F_{25} \geq 27.5$ Jy, and 18 sources in the MSX IRAS Gaps survey with MSX $F_{25} \geq 27.5$ Jy. Thus our initial list is dominated by stars selected by the 2MASS criteria. These lists were merged together to make a single target list, containing 21,335 sources. To merge the 2MASS and IRAS/MSX lists, we used a $60''$ matching radius. If more than one 2MASS source was within $60''$ of the IRAS position, we assumed the brightest K band source was the match.

Note we did not include sources in our input list based on their 60 and/or 100 μm IRAS flux densities, as extended emission from cirrus becomes more significant at these wavelengths. This means that the DIRBE Point Source Catalog is biased against very cold objects, such as galaxies and molecular clouds. Since we only used the point source catalogs of 2MASS, IRAS, and MSX for source selection, our sample is also biased against extended objects. Note also that we are only targeting sources bright enough to detect their possible variability in the DIRBE database (i.e., sources that may be detected in a *single* DIRBE scan at at least one DIRBE wavelength). By coadding the full light curves, it may be possible to detect fainter objects in the DIRBE database, but without variability information and with a higher likelihood of confusion. Such co-addition is beyond the scope of the current Catalog.

3. Extraction of the DIRBE Light Curves and the Catalog

For all 21,335 sources in our list, we extracted light curves at all ten wavelengths from the DIRBE Calibrated Individual Observations database. This database contains the individual calibrated 1/8th second samples taken in science-survey mode during each day of the DIRBE cryogenic mission. For all scans that pass within $0.3°$ of the target position, a linear baseline is fit to the sections $\pm 1.35° - 2.25°$ from the point of closest approach. The point source photometry is obtained by subtraction of this baseline and correcting for the DIRBE beam response. The uncertainties in the point source photometry are calculated as the root sum square of the rms noise of the baseline, the photometric error produced by a $1'$ error in the in-scan and cross-scan directions, an error due to short-term detector gain variations, and signal-dependent detector noise. The number of individual measurements per light curve ranges from 99 to 1932; the average and median number of data points per light curve are 488 and 423, respectively. The average uncertainties per measurement in the raw $1.25 - 240$ μm light curves are 33, 38, 27, 21, 107, 256, 1567, 3207, 8100, and 4510 Jy, respectively.

The COBE DIRBE Point Source Catalog (Table 1[1]) contains the time-averaged DIRBE flux densities F_ν in the ten DIRBE bands for all 11,785 sources in our initial list that had a flux at minimum in the weekly-averaged light curve in *any* of the six shortest DIRBE wavelengths greater than 3$\times$ the average noise per datapoint, plus three additional sources (see Section 6). These flux densities were calculated after filtering the light curves (see Section 5). The name of the object in the Catalog it was originally selected from is also given (IRAS/MSX and/or 2MASS) in Table 1. Table 1 also contains the number of individual measurements N available after filtering the light curves, the average uncertainty per measurement $<err>$, and the standard deviation $\sigma = \sqrt{\Sigma(F_i - <F>)/(N-1)}$ of the individual flux measurements F_i. Table 1 also gives the observed amplitude Δmag, the uncertainty assigned to that amplitude $\sigma(\Delta mag)$ (see Section 7 for definitions), and the confusion flags (see Sections 4 and 5 for definitions). The positions given in Table 1 (and the positions used for the extraction) came from either the 2MASS catalog or the IRAS/MSX catalog, with the 2MASS position preferentially used if available. No color corrections have been applied to the data in Table 1 (see Hauser et al. (1998) and Smith (2003) for a discussion of color corrections). The complete filtered light curves for variable sources will be published in a follow-up paper.

4. Flagging for Confusion

For each wavelength, three different confusion flags may be set in the DIRBE Point Source Catalog (see Table 2 for a summary of the flags and Table 3 for some basic statistics on the DIRBE Catalog, including statistics on flagging and number of sources detected

---

[1]Table 1 is only available in electronic form, at the Astrophysical Journal Supplement web site at http://www.journals.uchicago.edu/ApJ

above 3σ at each wavelength). The first confusion flag is set when a second known infrared-bright source is located within 0.5° of the target source. We used limits for the brightness of the companion of 25, 20, 20, 10, 30, 55, 320, and 765 Jy for $1.25 - 100$ μm, respectively. These are conservative limits, equal to the average per-measurement 1σ noise levels of the DIRBE light curves in Smith et al. (2002). At 1.25 and 2.2 μm, we used the 2MASS database to search for companions, while at 12 and 25 μm we used the IRAS Point Source Catalog and the IRAS Small Scale Structure Catalog (Helou & Walker 1985). At 3.5 μm, where there is no previous all-sky survey, we used the Catalog of Infrared Observations (Gezari, Pitts, & Schmitz 2000)[2], a compilation of all published infrared observations available in 1997. At 4.9 μm, we used both the Catalog of Infrared Observations and the synthetic all-sky 4.2 μm catalog of Egan & Price (1996), a list of estimated 4.2 μm flux densities for 177,860 stars created by extrapolation from the IRAS catalogues, other infrared catalogues, and optical measurements. Objects with companions above these flux limits were flagged at the respective wavelength in Table 1. The numbers of sources with companions in the DIRBE beam above the DIRBE noise level for each wavelength are given in Table 3. Note that this flagging may be incomplete at 3.5 and 4.9 μm, where no all-sky catalog is available. An additional uncertainty in the flagging may exist because the companion may be variable.

To help the Catalog user assess the relative contribution to the DIRBE flux density from the companion compared to the target source, in Table 4[3] we give the 2MASS and/or IRAS/MSX photometry of the target source, while in Table 5[4] we provide the names of

---

[2]Available from the VizieR service at http://vizier.u-strasbg.fr/viz-bin/VizieR

[3]Table 4 is only available in electronic form, at the Astrophysical Journal Supplement web site at http://www.journals.uchicago.edu/ApJ

[4]Table 5 is only available in electronic form, at the Astrophysical Journal Supplement

the companions, their 2MASS/IRAS/CIO/Egan & Price (1996) flux densities, and the distances between the companions and the target sources. In some cases the companion's flux density is small compared to that of the target source; in other cases, the companion dominates (see Sections 11 and 13 for examples).

Note that when two IRAS and/or two 2MASS sources in our input list are within a single DIRBE beam, they are both included in the DIRBE Catalog as separate listings, each flagged for a companion. In the DIRBE Catalog itself, we do not deconvolve the DIRBE flux of confused sources into that of the two sources, however, the information available in Tables 4 and 5 may help the Catalog user estimate the relative importance of each source to the DIRBE flux. As noted above, when both an IRAS and a 2MASS counterpart are listed in Table 1, this association is based solely on a positional offset of $\leq 1'$. It is possible that in some cases the IRAS and 2MASS sources are two different objects; with the DIRBE data alone, it is impossible to discriminate between them. Also note that an IRAS counterpart to a 2MASS source is only included if there is an IRAS source within $1'$ of the 2MASS source brighter than our IRAS selection criteria, and vice versa. Tables 1 and 4 do not list possible associations with IRAS or 2MASS sources fainter than our initial flux limits.

As an additional test for confusion, we compared the DIRBE photometry with that of 2MASS at 1.25 and 2.2 μm, and with that of IRAS at 12, 25, 60, and 100 μm. If the DIRBE flux density at minimum (after averaging in one-week periods) is more than 3σ larger than the 2MASS or IRAS flux densities at that wavelength, a second flag is set in Table 1. Since the DIRBE 0.7° beam is much larger than apertures used in 2MASS ($3''$ – $14''$) and the IRAS beams ($<8'$), discrepant fluxes may indicate a second source in the DIRBE beam or the presence of extended emission around the source. Alternatively, it may be due to large-amplitude or long time-scale variability. This second flag was also set

web site at http://www.journals.uchicago.edu/ApJ if the DIRBE maximum is less than a previous measurement minus 3σ. In Table 3, we provide statistics on the number of sources per wavelength that have this second flag set. The Catalog of Infrared Observations and the Egan & Price (1996) catalog were excluded from this comparison because of possible large uncertainties in the photometry, thus this flag was not set at 3.5 and 4.9 μm. This flag was also not set at 140 and 240 μm, since no all-sky catalogs are available at those wavelengths.

5. Filtering of the Light Curves

Another issue is the possibility of more distant companions, outside of the main DIRBE beam, affecting the 'sky' fluxes used in the photometry extraction. Inspection of the DIRBE data showed that, if a second infrared-bright star is between about 0.5° – 2.5° of the target star and if a scan happened to pass near that second star, flux from the nearby star sometimes contributed to the 'sky flux' used to calculate the photometry for the target source, causing erroneous photometry with large errorbars for the targeted star. Fortunately, however, scans in other directions were not affected by the second star. To correct for this problem, we filtered our data to remove scans affected by nearby stars. We searched previous infrared catalogs for objects within 3.2° of each targeted source. At each wavelength, for each DIRBE scan for each targeted source, we scaled the companion's flux density by a Gaussian with FWHM 0.7°, weighted by the minimum distance between the scan and the companion star. If the weighted flux density of the companion in the respective band was greater than 25, 20, 20, 10, 30, 55, 320, and 765 Jy at 1.25 – 100 μm, respectively, then the scan was removed from consideration. We also used the IRAS Small Scale Structure Catalog (Helou & Walker 1985) in this filtering process, since extended sources outside the DIRBE beam may also affect the DIRBE photometry.

The remaining measurements with large error bars ($\geq$3 times the average uncertainty) were likely affected by a cosmic ray hit in the 'sky' portion of the measurement. These large deviations were removed from the light curves by an additional filtering process. Generally, only a few DIRBE scans per light curve were removed by this additional filtering processing. A cosmic ray hit near the star itself may not produce a large error bar, but instead may manifest itself as a very discrepant flux measurement with a small error bar. We also removed these points from the final light curves. No all-sky catalogs are available at the two longest DIRBE wavelengths, thus these light curves were just filtered for measurements with large errors or very discordant photometry.

In some cases, filtering dramatically improved the DIRBE light curves, removing discrepant data points and those with large errorbars. Some example DIRBE light curves before and after filtering are shown in Figure 1 and in Smith (2003). The filtered light curves show much less scatter than the originals. In the case of the 1.25 μm light curve of IK Tau (Figure 1), the datapoints that were removed by filtering systematically had lower apparent flux densities than those at similar times that were not filtered. The filtering routine found six stars near IK Tau with 2MASS $F_{1.25\mu m}$ between 55 and 62 Jy, similar to the deviations seen in the datapoints that were removed. In the case of the 2.2 μm light curve for CW Leo (Figure 1), some very discrepant points with large error bars have been removed. These were caused by R Leo, which is $3'$ away from CW Leo. R Leo has 2MASS $F_{2.2\mu m}$ = 5505 Jy, similar to the deviations seen in the unfiltered light curve. In the case of the 12 μm light curve of R Leo, the discrepant points were caused by CW Leo, which is much brighter than R Leo at 12 μm, varying between $\sim$20,000 Jy and $\sim$ 40,000 Jy. Note that the bad scans occur at the same time for R Leo and CW Leo, as expected. The scans that were not removed by filtering had position angles such that they did not pass directly through both R Leo and CW Leo.

The filtering process somewhat reduces the average noise level in the light curves. Over the entire Catalog, the average noise levels in the filtered light curves are 30, 7, 17, 7, 18, 32, 118, and 468 Jy at 1.25 μm to 100 μm, respectively.

Because of incompleteness and photometric uncertainties in the comparison catalogs, and the fact that some of the nearby stars may themselves be variable, the flagging and filtering routines are not always perfect. To test for possible residual effects from companions in the final filtered light curves, we compared the average photometric uncertainty $<err>$ with the rms σ for two-week intervals in the light curves. Since the majority of variable stars in our sample are expected to be long-period variables (see Smith (2003)), small time-scale variations in the light curves are probably due to a nearby star affecting some scans more than others. If the $\sigma/<err>$ was greater than 3 for any two week period containing at least 10 measurements, a third confusion flag was set in Table 1. The number of sources with this flag set at each wavelength is given in Table 3. Note that the wavelength with the most sources with this flag set is 3.5 μm, because of the lack of an all-sky catalog for filtering purposes.

If a large fraction of the photometric values in a light curve were removed by filtering, the source may be confused. If the light curve of a source has fewer than about $50-100$ measurements in its light curve after filtering, then the photometry and variability parameters in the DIRBE Catalog should be considered somewhat suspect. In some cases, if a source is very confused, all of the scans at a wavelength were deemed affected by nearby companions, and so were filtered out. In these cases, no detection is recorded at that wavelength (specifically, the flux density is set to -99.9).

6. Completeness of the DIRBE Catalog Input List and the Catalog Itself

Our procedure of selecting sources from the IRAS, 2MASS, and MSX databases ensures that the input list for the DIRBE Catalog should be as complete as these catalogs for bright objects at high Galactic latitudes. At $|b| > 5°$, we estimate completeness limits of approximately 90, 60, 90, and 165 Jy at 1.25, 2.2, 12, and 25 μm, respectively, corresponding to magnitude limits of ∼3.1, 2.6, −1.3, and −3.5. These are 3.3×, 8.6×, 5.0×, and 5.1× the average noise level per scan in the filtered light curves, and are 3.6× our 1.25 μm 2MASS selection criterion, 3.0× our selection criterion at 2.2 μm, and 6× our selection criterion at 12 and 25 μm. This means that all sources with amplitudes ≤1.4 magnitudes at 1.25 μm, ≤1.2 magnitudes at 2.2 μm, and ≤1.9 magnitudes at 12 and 25 μm are included in our sample, even if they were observed at minimum by 2MASS or IRAS/MSX and at maximum by DIRBE. These amplitude limits are larger than typical values for Miras (see Section 12 and Table 17).

The DIRBE Catalog input list should also be complete at high Galactic latitudes at 3.5 μm to about 60 Jy, 3.5 × the average noise level in the filtered light curves. The reddest stars in K − L (i.e., $F_{2.2}/F_{3.5}$) in the Smith (2003) sample are the Mira carbons, with $F_{2.2}/F_{3.5} \sim 0.45$, $F_{3.5}/F_{4.9} \sim 0.61$, and $F_{4.9}/F_{12} \sim 0.88$. If these stars have $F_{3.5} = 60$ Jy they will have $F_{2.2} \sim 27$ Jy ($K \sim 3.47$), and thus would be included in the sample based on the 2.2 μm criterion ($K \leq 3.81$). Carbon Miras fainter than ∼44 Jy at 3.5 μm will not meet the 2.2 μm selection criterion, however, they are expected to be selected by the 12 μm criterion down to $F_{3.5} = 10$ Jy. Thus the DIRBE catalog input list should be complete at high Galactic latitudes at 3.5 μm to at least 60 Jy for sources with amplitudes ≤ 1.9 magnitudes. All of the sources in the DIRBE Catalog have smaller 3.5 μm amplitudes than this limit (see Section 12).

At 4.9 μm, we estimate a high latitude completeness limit of 50 Jy, 5× the average noise level at this wavelength. A carbon Mira with $F_{4.9}$ = 50 Jy has an expected F_{12} = 57 Jy, well above our IRAS 12 μm selection cut-off of 15 Jy. Thus all sources with 4.9 μm amplitudes of $\leq$1.4 magnitudes would be included in our sample to a limit of 50 Jy.

To confirm these estimates of the completeness limits of our input list, we performed three tests. First, to search for missing sources, we cross-correlated our input list of 21,335 sources with the 4.3 μm sources in the MSX IRAS Gaps survey (the 4% of the sky missed by IRAS with $|b| \geq 6°$; Egan et al. (1999)), the synthetic 4.2 μm catalog of Egan & Price (1996), and the Catalog of Infrared Observations at 3.5 and 4.2 $-$ 4.9 μm. There were no sources in the MSX IRAS Gaps survey with MSX band B1 (4.22 $-$ 4.36 μm) or band B2 (4.24 $-$ 4.45 μm) flux densities greater than our nominal completeness limit of 50 Jy which were not in our DIRBE input list, and only 8 with flux densities $\geq$ 30 Jy. All of these sources had very low quality detections in MSX band B1 (quality flag = 1; see Egan et al. (1999)) with $F_{B1} \leq$ 41 Jy, and were not detected in MSX band B2. We extracted DIRBE photometry for these 8 sources. None of them were detected at any wavelength by DIRBE.

Only 16 sources in the synthetic Egan & Price (1996) catalog have estimated 4.2 μm flux densities greater than 50 Jy, $|b| \geq 5°$, and are not in our initial source list for the DIRBE Catalog. We extracted DIRBE photometry for these 16 sources. None were detected by DIRBE at 4.9 μm.

At 3.5 μm, all but four of the high latitude ($|b| \geq 5°$) sources in the Catalog of Infrared Observations with $F_{3.5}$ greater than our nominal completeness limit of 60 Jy are included in our sample. At 4.9 μm, the DIRBE catalog input list does not include 181 of the 4.2 $-$ 4.9 μm high latitude sources in the Catalog of Infrared Observations brighter than 50 Jy. Nearly all of these apparent 'missing' sources are low S/N unconfirmed detections in the AFGL or TMSS, and thus may be spurious or extended sources, or have large positional errors. We extracted the DIRBE light curves for these positions, and found only one unconfused detection above 50 Jy at 4.9 μm. This source, the very bright star θ Cnc, was missed by 2MASS because it was strongly saturated. This star was also detected by DIRBE above our nominal completeness limits at 1.25, 2.2, and 3.5 μm. Another source, the semi-regular variable V1888 Cyg, was only detected at 4.9 μm by DIRBE, with a time-averaged flux density of 34.6 Jy, below our nominal Catalog completeness limit. These two sources were added to the DIRBE Point Source Catalog.

We also added RAFGL 2688 (the Egg Nebula) to the Catalog. This very dusty source lies in the small part of the sky not observed by either IRAS or MSX, but was strongly detected by DIRBE (see Section 14 and Figure 9b). These three additions bring the number of sources in the Catalog up to 11,788.

We note that infrared-bright transient objects would be missed by our sample selection criteria. For example, the Catalog of Infrared Observations contains three novae with 3.5 μm flux densities greater than our nominal completeness limit of 60 Jy, and two with 4.2 μm flux densities greater than our nominal 4.9 μm completeness limit of 30 Jy. In addition, SN1987A was detected at 4.2 μm above 30 Jy in the months following its appearance (Bouchet et al. 1989), but had faded significantly by the time of the DIRBE mission (Wooden et al. 1993), and was not detected by DIRBE.

As a second test of the completeness of the DIRBE Catalog input list, for a selected region of the sky we extracted DIRBE light curves for a much more sensitive sample of 2382 2MASS sources, covering $\sim$2% of the sky. This deeper sample had a 2MASS K band limit of $F_{2.2}$ = 1.4 Jy (K $\leq$ 6.7) (0.02 $\times$ the average noise level in the filtered DIRBE light curves) or $F_{1.25}$ = 12 Jy (J $\leq$ 5.3) (0.4 $\times$ the DIRBE per-point uncertainty), R.A. $\leq 0^{h}\ 30^{m}$, $|b| \geq 5^{\circ}$, and all Declinations. None of these additional sources have unconfused DIRBE time-averaged flux densities greater than our nominal completeness limits. This indicates that our initial selection criteria provides a very complete sample above these limits.

To further investigate the completeness levels of the Catalog, in Figure 2 we have plotted log N−log S at each wavelength for high Galactic latitudes ($|b| \geq 5^\circ$). At 1.25 − 25 μm, clear turn-overs are visible in these plots at flux levels of ∼40, 40, 40, 25, 65, and 110 Jy, respectively. These are somewhat lower than our nominal completeness limits, showing that our completeness estimates are reasonable. The log N−log S plots for 60 − 240 μm do not show turn-overs, showing that, as expected, the Catalog is not complete at those wavelengths.

Our estimated completeness limits only pertain to unconfused sources; as noted earlier, in some cases all of the measurements in a light curve are filtered out (see Section 5 and Table 6). Since filtering does not depend upon the brightness of the target source, the lack of photometry for these sources in the Catalog will lower the log N−log S curve, but should not strongly affect the turn-over flux density. To investigate the incompleteness of the Catalog itself due to this filtering, we searched the DIRBE Catalog input list for sources with 2MASS or IRAS/MSX photometry brighter than our nominal completeness limit at a given wavelength, which had all their measurements at that wavelength removed by filtering. In Table 6, we provide statistics on the resulting incompleteness of the Catalog. Approximately one quarter of the photometry is lost at 1.25, 2.2 μm, and 12 μm due to filtering, about half at 25 μm, about three quarters at 60 μm, and ∼85% at 100 μm.

This removal of all measurements by filtering is a strong function of Galactic latitude, in that it is more likely to happen at lower latitudes. In Figure 3, using equal sky-area bins, we plot, as function of Galactic latitude, the fraction of sources in our input list with 2MASS/IRAS/MSX fluxes above our nominal completeness limits that have had all their measurements removed by filtering. The worst cases are for 1.25 μm and 2.2 μm, where ∼65% of the photometry is lost at $|b| \leq 5^\circ$, decreasing to less than 10% at $|b| > 30^\circ$.

The resulting incompleteness of the Catalog at 1.25 μm and 2.2 μm is also visible in

Figure 4, where we plot a histogram of the number of sources in the Catalog as a function of Galactic latitude in equal sky-area bins. There are clear turn-overs of the 1.25 μm and 2.2 μm source counts at $|b| \sim 20°$, showing incompleteness below these latitudes.

In Figure 4, we also plot the number of flagged sources as a function of latitude, while in Figure 5, we give the fraction of Catalog sources that are flagged as a function of Galactic latitude. At $1.25 - 4.9$ μm, this fraction decreases with increasing latitude. The most extreme case is that of 2.2 μm, where 95% of sources with $|b| < 5°$ are flagged, and ∼40% at $|b| \geq 45°$. At 12 and 25 μm, the percentage of flagged sources is highest at $|b| \leq 5°$, but there is little correlation with latitude otherwise.

7. The DIRBE Variability Parameters

As noted in Section 3, in addition to the time-averaged infrared flux densities, Table 1 also includes both the standard deviation σ of the individual flux values in the light curve of the object (after filtering) and the mean uncertainty $<err>$ of the individual data points in the light curve. The comparison of these two values provides an estimate of the likelihood of variability of the object. In addition, for each light curve with minimum flux density greater than three times the average uncertainty per measurement, Table 1 also includes the total *observed* amplitude of variation during the DIRBE observations $\Delta mag = 2.5 log(F_{max}/F_{min})$, where F_{min} and F_{max} are the minimum and maximum flux densities after averaging over one week time intervals. Table 1 also lists $\sigma(\Delta mag)$, the uncertainty on Δmag, calculated from $\sigma(\Delta mag) = 2.5\sigma_{F_{max}/F_{min}}/(2.303(F_{max}/F_{min}))$, where $\sigma_{F_{max}/F_{min}}/(F_{max}/F_{min}) = \sqrt{(\sigma_{F_{max}}/F_{max})^2 + (\sigma_{F_{min}}/F_{min})^2}$ and $\sigma_{F_{max}}$ and $\sigma_{F_{min}}$ are set equal to the average uncertainty per measurement $<err>$. If the S/N at minimum in the weekly-averaged light curve was less than 3 then an amplitude and amplitude uncertainty were not calculated (that is, they were set to -99.9 in Table 1). We note that the observed changes in brightness given in the DIRBE Catalog may not represent the full range of variation for these stars, because many of the light curves are not complete and may not cover a full pulsation period. In these cases, the observed variations are a lower limit to the true amplitudes of variation. In Table 3, we list the numbers of unflagged sources at each wavelength with at least 100 measurements in their filtered light curves and $\Delta(\mathrm{mag})/\sigma(\Delta\mathrm{mag}) \geq 3$.

The largest unconfused DIRBE amplitudes are 2.2 magnitudes at 1.25 μm for the oxygen-rich Mira star IK Tau (see Figure 1), 1.8 and 1.6 magnitudes at 2.2 and 3.5 μm, respectively, for the carbon star CW Leo (see Figure 1), 1.5 magnitudes at 4.9 μm for the Mira star IZ Peg (see Figure 6), and 1.2 and 1.0 magnitudes at 12 and 25 μm, respectively, for the OH/IR star OH 348.2-19.7 (see Smith (2003)).

8. DIRBE vs. 2MASS Photometry

Stars brighter than J $\sim$ 4.5 ($F_{1.25\mu m} \sim$ 25 Jy) and K $\sim$ 3.5 ($F_{2.2\mu m} \sim$ 26 Jy) were saturated in 2MASS, thus their 2MASS photometry is somewhat uncertain ($\sigma \sim 0.2 - 0.3$ magnitudes; Cutri et al. (2003)). This means that for the brightest stars in the sky, DIRBE provides more accurate photometry at these wavelengths for unconfused sources. In Figure 7, we plot the distribution of the 2MASS and DIRBE 1.25 and 2.2 μm uncertainties for the subset of 791 sources in the DIRBE Catalog with 2MASS K < 1.0 (i.e., $F_{2.2} >$ 266 Jy). There is a dramatic difference, with the median 1.25 μm uncertainty in DIRBE being 0.03 magnitudes, and the median in 2MASS being 0.26 magnitudes. At 2.2 μm, the median DIRBE uncertainty is 0.02 magnitudes, and the median 2MASS uncertainty is 0.23 magnitudes. Thus for the brightest near-infrared sources, the DIRBE photometry is $\sim$10 times more precise than that of 2MASS.

In Figure 8a, we plot the 2MASS J magnitudes against the DIRBE 1.25 μm magnitudes for all unflagged $|b| \geq 5°$ sources in the DIRBE Catalog. In Figure 8b, we compare the 2MASS K magnitudes with the unflagged DIRBE photometry. For the unflagged sources in the K $<$ 1 subset, the best-fit relationships between the 2MASS and DIRBE photometry are $J_{DIRBE} = (1.011 \pm 0.010)J_{2MASS} - 0.019 \pm 0.016$ ($\chi^2 = 220$ with $N = 373$) and $K_{DIRBE} = (1.010 \pm 0.012)K_{2MASS} + 0.085 \pm 0.011$ ($\chi^2 = 154$ with $N = 389$). For the full Catalog, the best-fit relationships for the unflagged sources are $J_{DIRBE} = (0.937 \pm 0.003)J_{2MASS} + 0.077 \pm 0.012$ ($\chi^2 = 4304$ with $N = 4691$) and $K_{DIRBE} = (0.982 \pm 0.004)K_{2MASS} + 0.109 \pm 0.004$ ($\chi^2 = 3542$ with $N = 5169$). No sources were flagged for discrepant photometry from 2MASS that were not already flagged for a companion in the beam or $\sigma/<err> \geq 3$ in a 2-week period.

DIRBE also provides information about near-infrared variability, which is unavailable from 2MASS. In Table 7, we provide statistics on the DIRBE light curves and flagging for the 791 sources in the 2MASS K $<$ 1.0 sample. Of the 791 sources, 570 survive the filtering process at 2.2 μm (i.e., do not have all their measurements removed by filtering), and are detected in a single DIRBE scan at S/N $\geq$ 3. Of these 570 sources, 271 are unflagged at 2.2 μm, and have more than 100 points left in their light curves after filtering. Of these, 90 (33%) are observably variable at 2.2 μm ($\geq 3\sigma$ DIRBE amplitudes).

In Figure 9, we plot histograms of the observed DIRBE amplitudes at the six shortest DIRBE wavelengths for the sources in the K $<$ 1.0 subset. This plot only includes unflagged sources with high S/N light curves ($>3\sigma$ per scan) with at least 100 measurements remaining after filtering. The sizes of the bins at each wavelength are equal to the median uncertainty in the amplitude at that wavelength. These histograms, along with Table 7, show that the majority of the sources in this subset are not observably variable in the DIRBE data. For the sources that are variable, the observed amplitudes are all less than 2.5 magnitudes at

1.25 μm, less than 2 magnitudes at 2.2 μm and 3.5 μm, and less than 1.5 magnitudes at 4.9, 12, and 25 μm.

9. IRAS vs. DIRBE Variability

In Figure 10a, we plot the DIRBE 12 μm flux density against that from IRAS, for the unflagged $|b| \geq 5°$ sources. The DIRBE 25 μm flux densities for unflagged $|b| \geq 5°$ sources are plotted against the IRAS 25 μm flux density in Figure 10b. The errorbars plotted on the DIRBE flux densities are the standard deviations in the filtered light curves, thus they include both measurement errors and intrinsic variations. The best-fit lines to these data are $[\log F_{12}]_{DIRBE} = [0.979 \pm 0.014][\log F_{12}]_{IRAS} + 0.010 \pm 0.035$ ($\chi^2 = 431$, N = 149), and $[\log F_{25}]_{DIRBE} = [1.107 \pm 0.012][\log F_{25}]_{IRAS}$ - 0.135 ± 0.034 ($\chi^2 = 220$, N = 115).

Unlike the 2MASS Catalog, the IRAS Point Source Catalog provides variability information, in the form of the IRAS VAR parameter (see Beichman et al. (1988)). Sources that were detected in at least two detectors during a single IRAS scan were considered 'seconds-confirmed'. These seconds-confirmed detections were then 'hours-confirmed' by matching with detections in scans between 100 minutes to 36 hours later. These hours-confirmed measurements were then compared with other hours-confirmed detections on longer timescales (weeks to months) ('weekly-confirmed'). Typically two or three hours-confirmed measurements were obtained per object on the sky. The IRAS variability parameter VAR was obtained by comparing hours-confirmed measurements for sources with high or moderate quality fluxes at both 12 and 25 μm. For a source to be considered variable, fluxes at both 12 and 25 μm must have increased or decreased significantly from one hours-confirmed sighting to another (i.e., their variations must be correlated). For the VAR parameter to be set to 99 percent probability, a 2.6σ correlated change must have occurred at both wavelengths; for VAR = $50 - 98$ percent probability, a $0.9 - 2.6\sigma$

correlated change must have occurred. This means that sources with very long periods of variation may not have been flagged as variable in IRAS. In addition, if two hours-confirmed observations were made during approximately same variability phase, the object may not have been flagged as variable. Furthermore, since the amount of variation needed for a VAR $\sim$ 50% setting is relatively low, VAR values in this range are expected to be somewhat unreliable.

Because of the good temporal coverage of COBE, the DIRBE variability parameters, particularly the amplitude of variation compared to the uncertainty on the amplitude, are expected to be more reliable indicators of variability for high S/N unconfused objects. DIRBE has the extra advantage of additional shorter wavelength bands than IRAS.

In Figures 11a $-$ f, we compare the IRAS VAR parameter with the DIRBE amplitude of variation at the six shortest DIRBE wavelengths for the sources in the Smith (2003) sample (IRAS $F_{12} \geq 150$ Jy; $|b| \geq 5°$). We have excluded sources with less than 5σ DIRBE flux densities at minimum light at the given wavelength, sources that were flagged as possibly confused in the DIRBE database, and sources which were flagged in the IRAS Point Source Catalog as possibly being confused or in a region dominated by cirrus. We have only included sources with high quality IRAS fluxes at both 12 and 25 μm.

These plots show considerable scatter. In particular, a number of stars that have low IRAS VAR parameters have large amplitudes of variation in the DIRBE database (>0.5 magnitude). As expected, the IRAS satellite was unsuccessful in detecting variability for some strongly variable stars. DIRBE is also better at finding smaller variations than IRAS. This figure shows a number of sources that are variable in DIRBE (Δ(mag)/σ(Δ(mag)) > 3) with low amplitude (<0.4 magnitudes), but have low IRAS VAR. The DIRBE light curves of the stars variable in DIRBE but with low IRAS VAR have been inspected by eye, and confirmed that they are indeed variable in the DIRBE database. Most of these stars are well-known variable stars, including Mira, which has an IRAS VAR parameter of only 3.

Note, however, that the majority of VAR = 99 sources are strongly variable in the DIRBE database. In fact, most sources with VAR $\geq$ 80 are also variable in DIRBE. Thus using the IRAS VAR parameter to select highly variable sources (as in, for example, Allen, Kleinmann, & Weinberg (1993)) appears to be reasonably reliable (albeit incomplete).

10. Associations with Other Catalogs and Spectral Types

To obtain associations with known optical sources and sources at other wavelengths, the DIRBE Catalog was cross-correlated with the SIMBAD database (Wenger et al. 1996). The results are given in Table 8[5]. The closest source listed in SIMBAD within $1'$ was assumed to be the same source, and the spectral type and object type of this source are given in Table 8. SIMBAD sometimes has more than one listing for the same source, if the source appeared in two different catalogs with slightly different positions and different names. Therefore, if a second SIMBAD source is listed within $5''$ of the first source, that second source and its SIMBAD object type and spectral type are also given in Table 8. We also cross-correlated our list with the General Catalog of Variable Stars (GCVS; (Kholopov et al. 1985-1988)), the New Catalog of Suspected Variables (NSV; (Kukarin et al. 1982)), and the NSV Supplement (NSVS; Kazarovets & Durlevich (1998)), using search radii of $60''$, $30''$, and $5''$, respectively. If a match occurred, the variability type and period are included in Table 8, if available. Table 8 also includes IRAS spectral types from Kwok, Volk, & Bidelman (1997) for the IRAS sources. In addition, we compared our list with the Chen et al. (2001) OH/IR star compilation, which is listed by IRAS name. DIRBE Catalog sources

[5]Table 8 is only available in electronic form, at the Astrophysical Journal Supplement web site at http://www.journals.uchicago.edu/ApJ

that are in that list are noted in Table 8, and the OH expansion velocity is included.

Although the SIMBAD classifications are inhomogeneous and incomplete, they provide some rudimentary statistical information about the types of sources contained in the DIRBE Catalog. In Table 9, we provide statistics on types as a function of wavelength, for the sources with S/N per scan ≥ 3 at that wavelength. The sources have been divided into 18 groups, based on their SIMBAD spectral type and object type, as well as their variability type from the GCVS, NSV, or NSVS, if available. Stars with optical types M, K, S, and C are divided into two groups: those with variability types associated with the AGB (Mira, SRa, SRb, Lb), and those not previously classified into one of those variability types. Objects identified in SIMBAD, the GCVS, the NSV, or the NSVS as young stellar objects, Orion variables, Herbig Ae/Be stars, T Tauri stars, H II regions, or Herbig-Haro objects are lumped together as star formation sources. Sources listed in SIMBAD as post-AGB objects are also separated out, as are planetary nebulae, possible planetary nebulae, and galaxies. Stars with optical types of O, B, A, F, and G not included in one of these sets are tabulated separately. A similar listing for the 2MASS K $<$ 1.0 subsample is presented in Table 10. This near-infrared-bright subset has no known star formation sources, post-AGB objects, or planetary nebulae, but contains mainly late-type stars.

In addition to providing the number of sources of each type detected at each wavelength at S/N ≥ 3 per scan, in Tables 9 and 10 we give statistics on the number of these that are unflagged and have at least 100 measurements left after filtering. We also include the number of unflagged sources with ≥ 100 measurements that are variable with amplitude/σ-amplitude ≥ 3. Table 9 shows that, of the 2352 unflagged high S/N 4.9 μm sources, 984 were previously classified as Mira, SRa, SRb, or Lb. Of these, 152 (15%) are observably variable in the DIRBE database. Of the remaining 1368 not previously classified as one of these variability types, 70 (5%) are variable in DIRBE at the 3σ level. At 12

μm, 85 of 311 (27%) unflagged high S/N sources are variable; 42 of these (49%) are not previously classified as Mira, SRa, SRb, or Lb. Note that, of the unflagged carbon stars not previously classified as one of these variability types, more than half of the stars that are detected at 4.9, 12, or 25 μm are variable at these wavelengths.

11. The Brightest Catalog Sources

In Tables 11 – 16, the brightest 10 sources in the DIRBE Catalog at each of the six shortest wavelengths are given. Although these are the brightest sources in the Catalog, they are not necessarily the brightest sources in the sky because filtering eliminates some sources and because of incompleteness in the Galactic plane. The characteristics of the brightest sources change with wavelength. At the shortest wavelengths, optically-bright semi-regulars and non-variable K and M stars dominate. At the longer wavelengths, more evolved dusty stars and star formation regions become more important.

Some of these extremely bright sources are clearly variable in DIRBE. For example, see the 2.2 – 60 μm DIRBE light curves for W Hya shown in Figure 6 and the DIRBE light curves of CW Leo, α Ori, VY CMa, and L_2 Pup presented in Figure 1 and Smith (2003).

At 12 and 25 μm there is considerable confusion in the vicinity of star formation regions, such as that in Orion. This demonstrates the need for caution in using flagged photometry from the Catalog.

12. DIRBE Variability of AGB Stars

As shown in Table 9, the vast majority of objects in the DIRBE Catalog with known optical spectral types are late-type stars (spectral types M, K, S, and C). Of these, more than half are known variables with variability types associated with the AGB. In Smith et al. (2002) and Smith (2003), we showed that the amplitudes of variation for these types of stars tend to decrease with increasing wavelength. Further, the amplitudes increased along the sequence SRb/Lb −> SRa −> Mira. The DIRBE Catalog contains a significantly larger number of sources than these earlier studies, so we have repeated these analyses with the full Catalog sample.

In Table 17, we provide the mean DIRBE amplitudes of variation at each wavelength $<\Delta(mag)>$ for the known Miras, SRa, SRb, and Lb stars in the DIRBE Catalog. We have separated the stars into groups according to whether they are oxygen-rich (M stars and/or IRAS LRS types E or A; see Kwok, Volk, & Bidelman (1997)), carbon-rich (optical types C, N or R, or IRAS type C), optical type S (C/O ratio ~ 1), or known OH/IR stars (often also optical type M and/or IRAS type A or E). We also include the average uncertainty in the amplitude, $< \sigma(\Delta(mag)) >$. In constructing Table 17, we only included unflagged stars with $\geq 5\sigma$ DIRBE flux densities at minimum light.

In Table 18, we provide the mean ratios of the amplitudes at adjacent wavelengths for the different classes of objects. The quoted uncertainties in this Table are the standard deviations of the ratios for each class. Table 18 excludes flagged stars and stars with flux densities less than 5σ at minimum and $\Delta(\mathrm{mag})/\sigma(\Delta(\mathrm{mag})) < 5$ at either wavelength. These results are shown graphically in Figure 12, where we plot the mean amplitude ratio for two adjacent wavelength bands as a function of the shorter wavelength. Table 18 and Figure 12 show that, on average, there is a decrease in amplitude with wavelength, with the exception of the 4.9 μm/12 μm amplitudes for the oxygen-rich Miras, the 2.2 μm/3.5 μm amplitudes for the carbon Miras and the oxygen-rich SRb stars, and the 1.25 μm/2.2 μm amplitudes for the oxygen-rich SRa stars. There is, however, a lot of scatter in the amplitude ratios from star to star; although the average ratio tends to decrease with wavelength, for some individual stars the ratio increases or remains constant. This general trend is consistent with earlier DIRBE results with a smaller sample (Smith 2003) as well as ground-based studies (Harvey et al. 1974).

Such amplitude decrements with wavelength are predicted by theoretical models of AGB stars (Le Bertre 1988; Winters et al. 1994, 2000). A decrease in amplitude with wavelength means that the dust shell is redder at stellar minimum than at maximum. At any given radius in a circumstellar shell, the average dust temperature is expected to be highest at stellar maximum, and the radii that dust condensation and evaporation occur are largest at stellar maximum. Assuming a roughly $1/r^2$ density distribution for the dust in the shell and integrating over all of the dust in the shell, the optical depth of the shell is therefore highest at minimum, while the average effective dust temperature for the shell is lowest. This produces a redder infrared spectrum at minimum.

13. Massive Evolved Stars

In Smith (2003), we presented the DIRBE light curves of the supergiants α Ori and VY CMa. The dusty object VY CMa, the fourth brightest object in the DIRBE Catalog at 25 μm (Table 16), is variable in the mid-infrared, but not as variable as a typical Mira. Another object that may be similar to VY CMa is NML Cyg (V1489 Cyg) (Neugebauer, Martz, & Leighton 1965), also an OH/IR star and the thirteenth brightest 25 μm DIRBE Catalog source. NML Cyg may also be a supergiant (Johnson 1967; Morris & Jura 1983). NML Cyg is clearly variable in the DIRBE database (see Figure 13a), with observed amplitudes of 0.30 $\pm$ 0.03, 0.23 $\pm$ 0.06, and 0.20 $\pm$ 0.06 magnitudes at 3.5, 12, and 25 μm, respectively. These amplitudes are somewhat larger than those of VY CMa, but smaller than typical values for Miras (see Table 17).

Monnier et al. (1997) published a 10.2 μm light curve for 1980 – 1995 for NML Cyg, and found a period of ~940 days. Their photometry is consistent within the uncertainties with that of DIRBE for the time period in common. The DIRBE photometry and amplitudes are also reasonably consistent with the older data of Harvey et al. (1974) and Strecker (1975), as well as the IRAS time-averaged flux densities (from the xscanpi software) of F_{12} = 5461 Jy and F_{25} = 4065 Jy, and the MSX photometry (Egan et al. 1999).

14. Planetary Nebulae and Post-AGB Objects

Only 8 sources detected by DIRBE at the $\geq 3\sigma$ level per measurement at 4.9 μm are classified in SIMBAD as post-AGB objects, while 4 are listed as planetary nebulae or suspected planetary nebulae. None of these sources were found to be unconfused and variable at the $\geq 3\sigma$ level in DIRBE at any wavelength (Table 9). In Figure 13b, we show a few light curves for the post-AGB object RAFGL 2688 (the Egg Nebula), which is not variable in DIRBE.

15. An Object in Transition: OH 231.8+4.2 (QX Pup)

One of the most intriguing objects in the DIRBE Catalog is OH 231.8+4.2 (QX Pup), which apparently is in the process of changing from an AGB star to a post-AGB object (Meakin et al. 2003). OH 231.8+4.2 is a bipolar reflection nebula (Reipurth 1987) with an embedded M9III star (Cohen 1981). This star is known to be variable with an amplitude of approximately 2 magnitudes at 2.2 μm and a pulsation period of 700 days (Kastner et al. 1992), typical of Miras. This is thus a very unusual source, in a brief and rarely observed stage of development: a pulsating AGB star inside of a proto-planetary nebula.

OH 231.8+4.2 is variable in the DIRBE database, with an amplitude of 0.29 $\pm$ 0.07

magnitudes at 25 μm (see Figure 13c). This confirms the high IRAS VAR of 99 for this source. The DIRBE 25 μm amplitude for OH 231.8+4.2 is less than the average for the known Miras in the DIRBE Catalog (Table 17), which typically have amplitudes of 0.5 magnitudes at 25 μm, however, DIRBE may not have observed a full pulsation cycle for this star. OH 231.8+4.2 is also variable at longer wavelengths, with a measured amplitude of approximately 0.32 magnitudes at 850 μm (Jenness et al. 2002).

OH 231.8+4.2 is one of the reddest evolved stars in the DIRBE Catalog. In Figure 14, we plot the IRAS flux ratios for the 43 unconfused sources in the DIRBE Catalog with IRAS colors $F_{25}/F_{12} \geq 1.2$ and $F_{60}/F_{25} \leq 2.5$, and high quality IRAS fluxes at 12, 25, and 60 μm. These colors are in the range expected for very late AGB stars and post-AGB objects (van der Veen & Habing 1988). Using types from SIMBAD and additional information from the literature, in Figure 14 we use different symbols to identify young stars, post-AGB objects, planetary nebula, and OH/IR stars not identified as post-AGB objects. For comparison, we also mark the location of the post-AGB Egg Nebula (RAFGL 2688), based on its DIRBE data, and the variable supergiant NML Cyg, based on IRAS xscanpi results. Of these 45 objects, eight were found to be variable in the DIRBE database. These are distinguished by filled symbols in Figure 14.

In Figure 14, we also plot the regions defined by van der Veen & Habing (1988). As discussed by van der Veen & Habing (1988), sources in Regions II, IIIa, and IIIb are mainly AGB stars, with increasing circumstellar shell optical depth along this sequence. Region IV contains very late-stage AGB stars as well as some planetary nebulae. We also plot the theoretical evolutionary track for AGB stars of Bedijn (1987) in Figure 14. Stars get redder as they evolve, moving to the upper right on the IRAS color-color plot. After the stars evolve into region IV of the IRAS color-color plot, they move into Region V, which contains mainly non-variable objects, including planetary nebulae and post-AGB objects (van der

Veen & Habing 1988). OH 231.8+4.2 is the reddest source in this plot, lying in the extreme upper right of the color-color plot, to the right of region V, far from the standard AGB evolutionary track, and far from the other sources found to be variable in DIRBE.

16. Star Formation Regions and Other O, B, A, F, and G Stars

As shown in Table 9, 47 of the sources detected at the 3σ level at 4.9 μm in a single DIRBE scan are associated with star formation regions. Confusion is a major problem for the star formation sources in the Catalog; only 9 of these sources are unflagged. None of these are variable in DIRBE at a $\geq 3\sigma$ level.

Table 9 shows that 150 of the high S/N unflagged 4.9 μm sources in the DIRBE Catalog are O, B, A, F, or G stars, but are not previously identified as being associated with star formation regions or post-AGB objects. Of these sources, none are variable in DIRBE.

17. Galaxies

As noted above, the DIRBE Catalog selection criteria are biased against galaxies, since we are only selecting sources at wavelengths $\leq$ 25 μm and are biased against extended objects. Only two galaxies are included in the final DIRBE Catalog: M82 and NGC 253. Their IRAS flux densities fit our selection criteria, and they are detected at $\geq 3\sigma$ in a single DIRBE scan at 12 and 25 μm. As expected, their light curves show no evidence for variations. NGC 253 is also detected at 1.25 and 2.2 μm with average flux densities of 20 $\pm$ 4 Jy and 19 $\pm$ 6 Jy per measurement, consistent with values in the 2MASS Large Galaxy

Atlas[6] (Jarrett et al. 2003). By co-addition over the entire DIRBE mission, it is possible to detect additional galaxies at wavelengths of $\geq$60 μm (see Odenwald, Newmark, & Smoot (1998)). Such co-addition is beyond the scope of the current Catalog.

18. Summary

From the archival COBE DIRBE database, we have constructed a DIRBE Point Source Catalog containing 11,788 sources detected at the 3σ level per measurement at at least one DIRBE wavelength. This catalog was created using an input list of 21,335 IRAS/MSX and 2MASS sources. We have flagged sources likely to be confused, based on other infrared catalogs and inspection of the DIRBE light curves, and have collected information about the DIRBE sources from other catalogs. We compare the DIRBE photometry with that of 2MASS for the near-infrared-bright sources in the DIRBE Catalog, and show that the DIRBE photometry is more precise. We compare the DIRBE variability parameters with the IRAS VAR parameter, and show that DIRBE detected variability in a number of sources with low IRAS VAR. We also discuss a few unusual objects in the Catalog, including the peculiar bipolar nebula OH 231.8+4.2, likely evolving from the AGB into a post-AGB object.

We would like to thank the COBE team for making this project possible. We are especially grateful to the DIRBE Principal Investigator Michael Hauser. The DIRBE Calibrated Individual Observations data product was developed by the COBE Science Working Group and provided by the National Space Science Data Center at NASA's Goddard Space Flight Center. We appreciate the work of Nils Odegard, who wrote the first version of the DIRBE light curve extraction routine. We also thank the referee, David

[6] Available at http://irsa.ipac.caltech.edu/applications/Gator/.

Leisawitz, for helpful comments that significantly improved this paper. We also thank Anatoly Miroshnichenko and Mark Giroux for helpful communications, and J. M. Houchins for computer support. This research has made use of the SIMBAD database, operated at the CDS, Strasbourg, France, as well as NASA Astrophysics Data System at the Harvard-Smithsonian Center for Astrophysics, the VizieR service at the CDS, Strasbourg, France, and the Infrared Science Archive, operated by the Jet Propulsion Laboratory, California Institute of Technology. We have also made use of the electronic versions of the General Catalogue of Variable Stars, the New Suspected Variable Stars Catalogue, and the Supplement to this catalogue, provided by the Sternberg Astronomical Institute at Moscow State University. This research was funded by National Science Foundation POWRE grant AST-0073853 and NASA LTSA grant NAG5-13079.

REFERENCES

Allen, L. E., Kleinmann, S. G., & Weinberg, M. D. 1993, ApJ, 411, 188

Bedijn, P. J. 1987, A&A, 186, 136

Beichman, C. A., Neugebauer, G., Habing, H. J., Clegg, P. E., & Chester, T. J. 1988, Explanatory Supplement for the Infrared Astronomical Satellite Catalogs and Atlases (Washington, D.C.: US GPO)

Boggess, N. W., et al. 1992, ApJ, 397, 420

Burdick, S. V., & Murdock, T. L. 1997, 'COBE Final Report: DIRBE Celestial Calibration', Technical Report, General Research Corporation, Danvers MA

Bouchet, P., Moneti, A., Slezak, E., Le Bertre, T., & Manfroid, J. 1989, A&AS, 80, 379

Chen, P. S., Szczerba, R., Kwok, S., & Volk, K. 2001, A&A, 368, 1006

Cohen, M. 1981, PASP, 93, 288

Cohen, M. 1998, AJ, 115, 2092

Cutri, R. M. 2003, Explanatory Supplement to the 2MASS All Sky Data Release

Egan, M. P., Price, S. D., Moshir, M. M., Cohen, M., & Tedesco, E. 1999, The Midcourse Space Experiment Point Source Catalog Version 1.2 Explanatory Guide, Technical Report, AD-A381933, AFRL-VS-TR-1999-1522

Danchi, W. C., Green, W. H., Hale, D. D. S., McElroy, K., Monnier, J. D., Tuthill, P. G., & Townes, C. H. 2001, ApJ, 555, 405

Egan, M. P., & Price, S. D. 1996, AJ, 112, 2862

Epchtein, N., et al. 1999, A&A, 349, 236 Matsuura, O. T., & Picazzio, E. 1987, A&AS, 71, 39

Gezari, D. Y., Pitts, P. S., & Schmitz, M. 2000, Catalog of Infrared Observations, version 5.1

Harvey, P. M., Bechis, K. P., Wilson, W. J., & Ball, J. A. 1974, ApJS, 27, 331

Hauser, M. G., Kelsall, T., Leisawitz, D., & Weiland, J. 1998, 'COBE Diffuse Infrared Background Experiment (DIRBE) Explanatory Supplement', V. 2.3.

Helou, G., & Walker, D. W. 1985, 'IRAS Small Scale Structure Catalog', (Pasadena: Jet Propulsion Laboratory; Joint IRAS Science Working Group)

IRAS Point Source Catalog 1988, Version 2, Joint IRAS Science Working Group (Washington: GPO).

Jarrett, T. H., Chester, T., Cutri, R., Schneider, S. E., & Huchra, J. P. 2003, AJ, 125, 525

Jenness, T., Stevens, J. A., Archibald, E. N., Economou, F., Jessop, N. E. & Robson, E. I. 2002, MNRAS, 336, 14

Johnson, H. L. 1967, ApJ, 149, 345

Kastner, J. H., Weintraub, D. A., Zuckerman, B., Becklin, E. E., McLean, I., & Gatley, I. 1992, ApJ, 398, 552

Kazarovets, E. V., & Durlevich, O. V. 1998, 'New Catalogue of Suspected Variable Stars Supplement', Version 1.0, IBVS No. 4655

Kholopov, P. N. et al. 1985-1988, General Catalogue of Variable Stars

Knapp, G. R., Pourbaix, D., Platais, I., & Jorissen, A. 2003, A&A, 403, 993

Kukarin, B. V. et al. 1982, 'New Catalogue of Suspected Variable Stars', (Moscow: Publication Office 'Nauka')

Kwok, S., Volk, K., & Bidelman, W. P. 1997, ApJS, 112, 557

Le Bertre, T. 1988, A&A, 190, 79

Little-Marenin, I. R. & Stencel, R. E. 1992, PASPC, 26, 591

Meakin, C. A., Beiging, J. H., Latter, W. B., Hora, J. L., & Tielens, A. G. G. M. 2003, ApJ, 585, 482

Monnier, J. D. et al. 1997, ApJ, 481, 420

Morris, M., & Jura, M. 1983, ApJ, 267, 179

Neugebauer, G., & Leighton, R. B. 1969, Two Micron Sky Survey, a Preliminary Catalogue (NASA SP-3047).

Neugebauer, G., Martz, D. E., & Leighton, R. B. 1965, ApJ, 142, 399

Odenwald, S., Newmark, J., & Smoot, G. 1998, ApJ, 500, 554

Olnon, F. M., Baud, B., Habing, H. J., de Jong, T., Harris, S., & Pottasch, S. R. 1984, ApJ, 278, L41

Price, S. D., et al. 1999, 'Astrophysics with Infrared Surveys: A Prelude to SIRTF', ASP Conference Series, V. 177, 394

Price, S. D. & Walker, R. G. 1976, Interim Report Air Force Geophysical Laboratory, Hanscom AFB

Reipurth, B. 1987, Nature, 325, 787

Smith, B. J., Leisawitz, D., Castelaz, M. W., & Luttermoser, D. 2002, AJ, 123, 948

Smith, B. J. 2003, AJ, 126, 935

Strecker, D. W. 1975, AJ, 80, 451

Van der Veen, W. E. C. J., & Habing, H. J. 1988, A&A, 194, 125

Wenger, M., et al. 1996, BAAS, 189, 602

Winters, J. M., Fleischer, A. J., Gauger, A., & Sedlmayr, E. 1994, A&A, 290, 623

Winters, J. M., Le Bertre, T., Jeong, K. S., Helling, C., & Sedlmayr, E. 2000, A&A, 361, 641

Wooden, D. H., Rank, D. M., Bregman, J. D., Witteborn, F. C., Tielens, A. G. G. M., Cohen, M., Pinto, P. A., & Axelrod, T. S. 1993, ApJS, 88, 477

This manuscript was prepared with the AAS LaTeX macros v5.0.

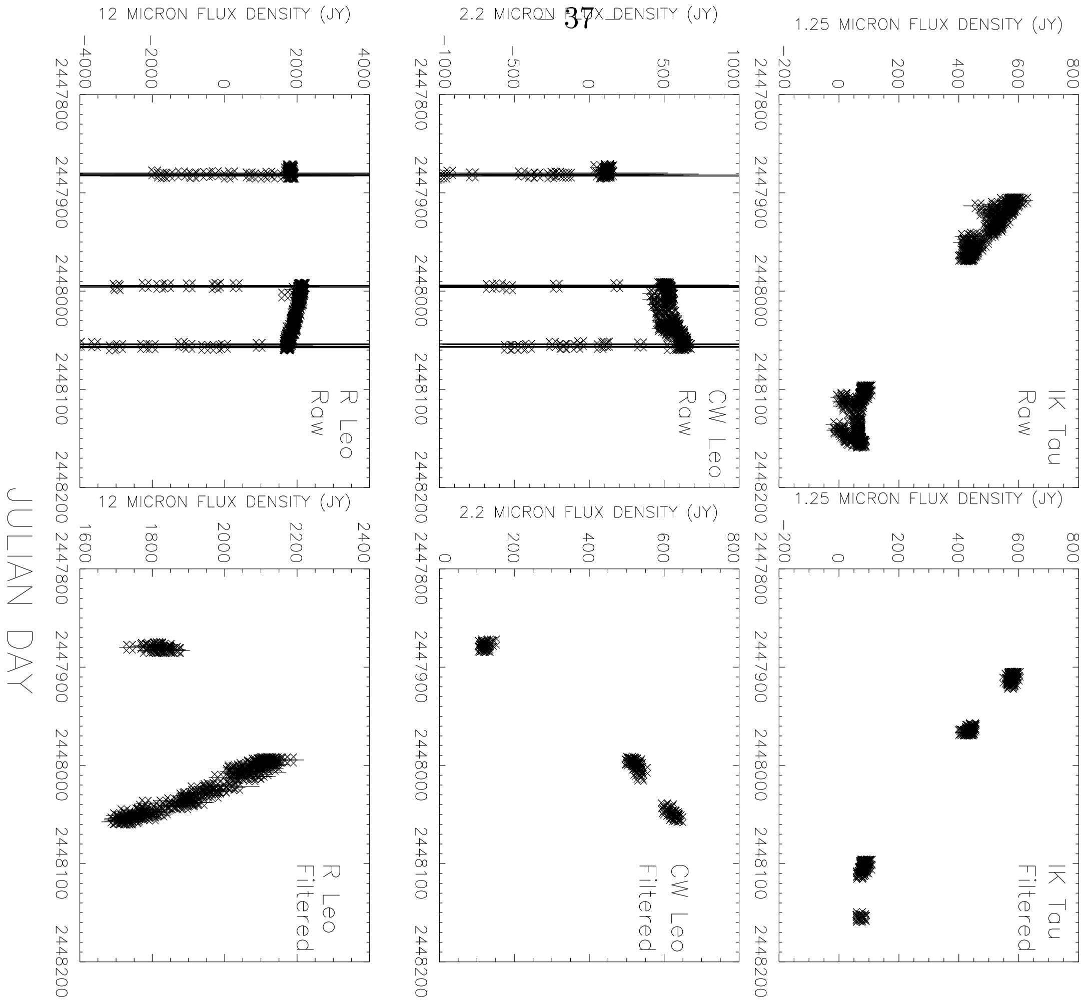

Fig. 1.— Some examples of light curve filtering. a) The raw 1.25 μm DIRBE light curve of IK Tau. b) The filtered 1.25 μm DIRBE light curve of IK Tau. c) The raw 2.2 μm light curve for CW Leo. d) The filtered 2.2 μm light curve for CW Leo. e) The raw 12 μm light curve of R Leo. f) The filtered 12 μm light curve of R Leo.

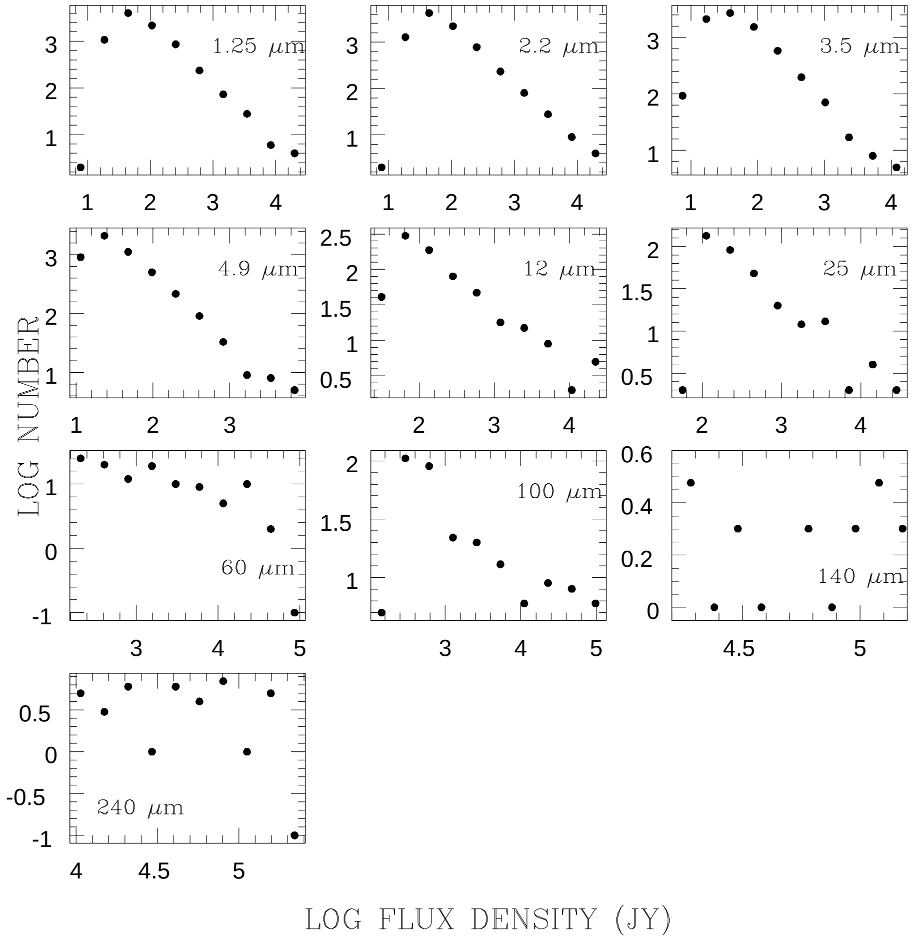

Fig. 2.— Log N − log S plots made from the DIRBE Point Source Catalog, for high Galactic latitude sources ($|b| \geq 5°$).

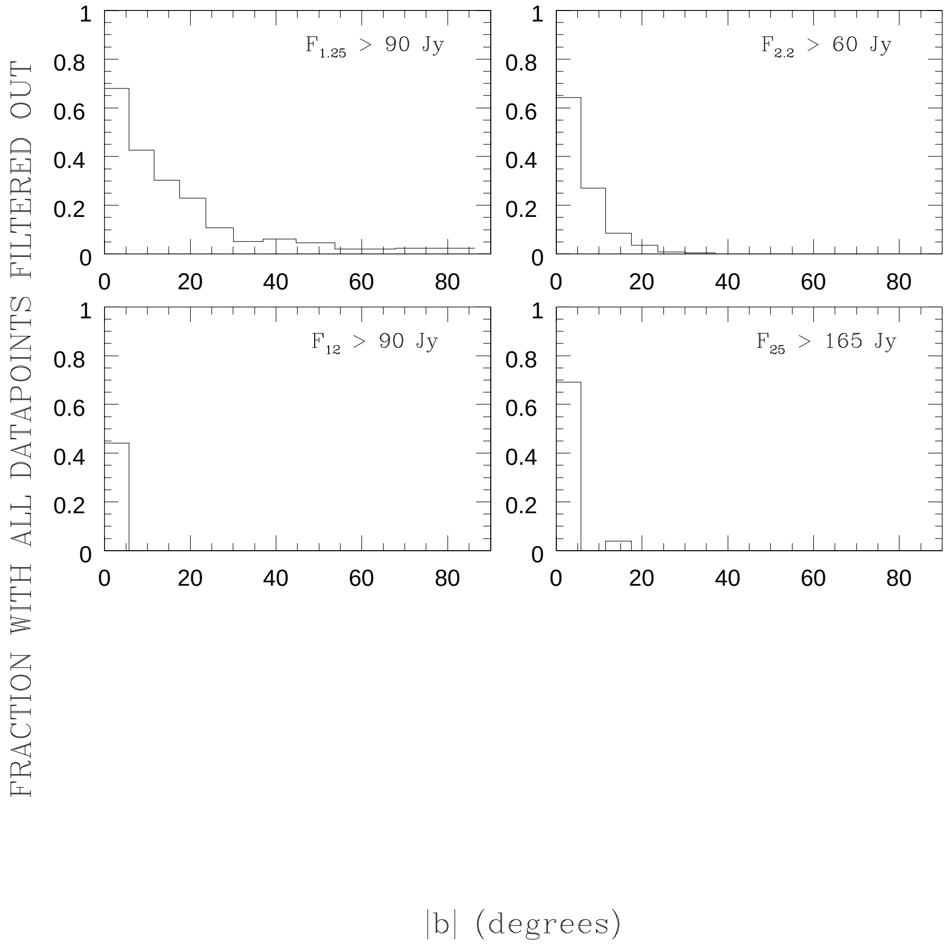

Fig. 3.— The distribution with Galactic latitude of the fraction of 1.25, 2.2, 12, and 25 μm sources with flux densities from 2MASS, IRAS, or MSX above the Catalog input list nominal completeness limits that have all their DIRBE measurements removed by filtering. The bins cover equal sky area.

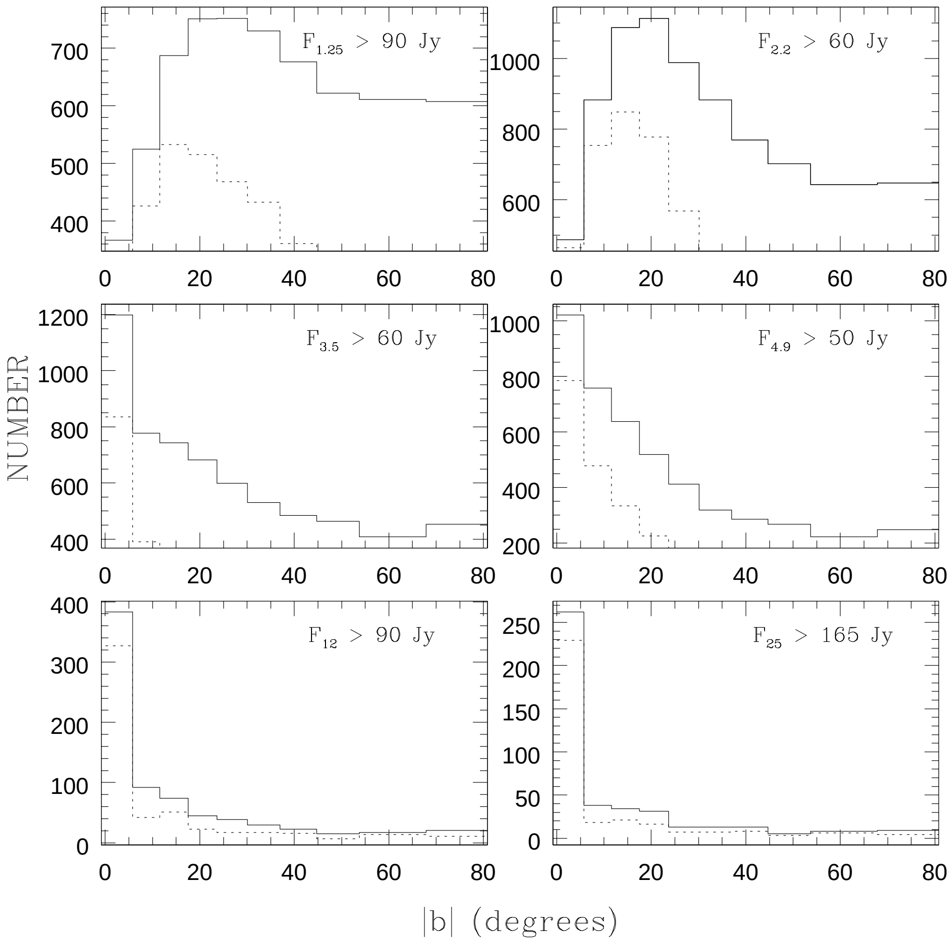

Fig. 4.— Solid line: A histogram of the number of sources in the DIRBE Catalog with DIRBE photometry above the Catalog input list nominal completeness limits. Dotted line: a similar histogram for the flagged sources. The bins cover equal sky areas.

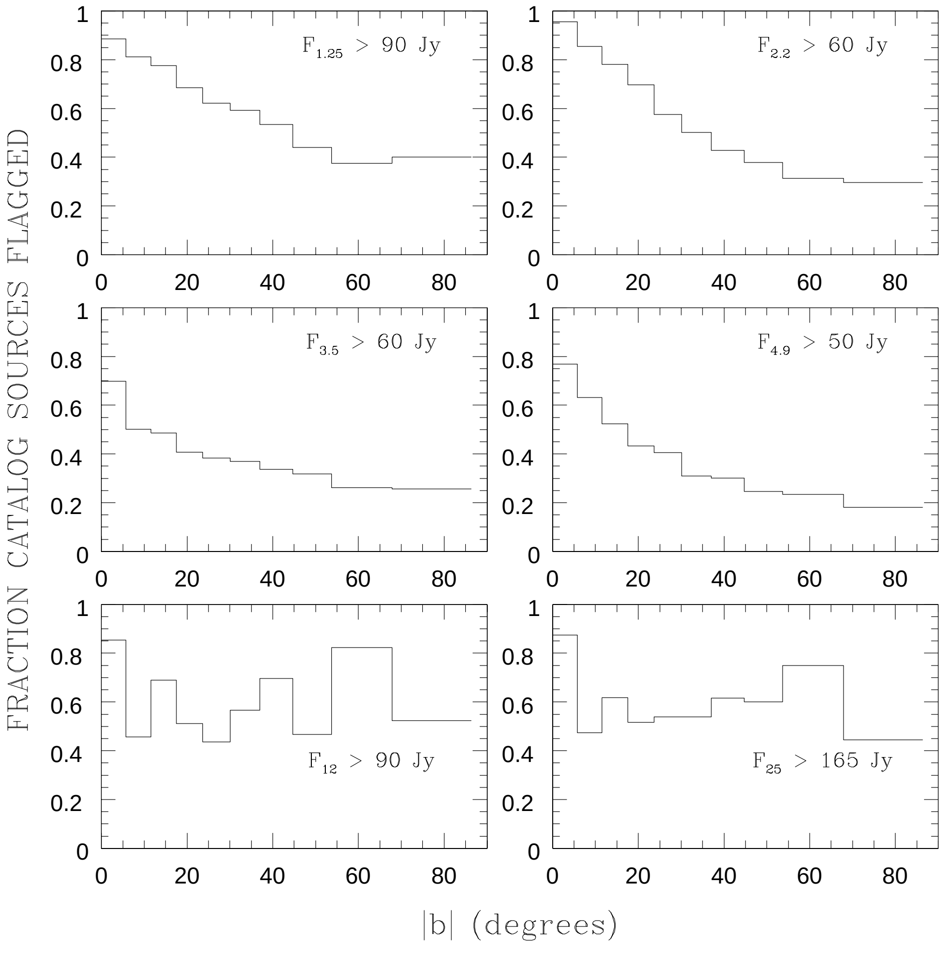

Fig. 5.— The fraction of flagged sources above the nominal completeness limits as a function of Galactic latitude. The bins cover equal sky area.

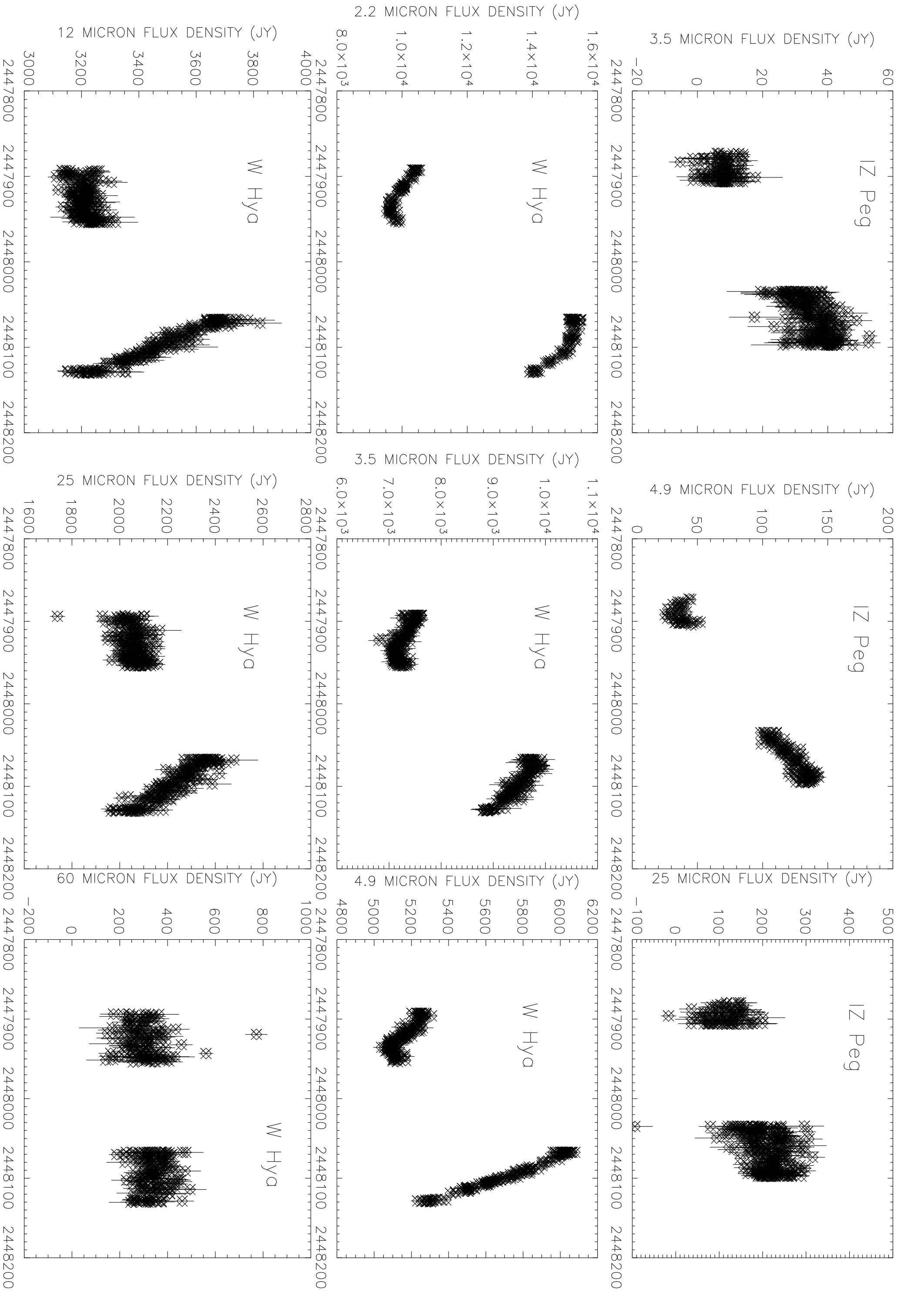

Fig. 6.— Some example light curves. Top row: DIRBE light curves at 3.5, 4.9, and 25 μm for IZ Peg. Middle and bottom row: DIRBE light curves at 2.2, 3.5, 4.9, 12, 25, and 60 μm for W Hya.

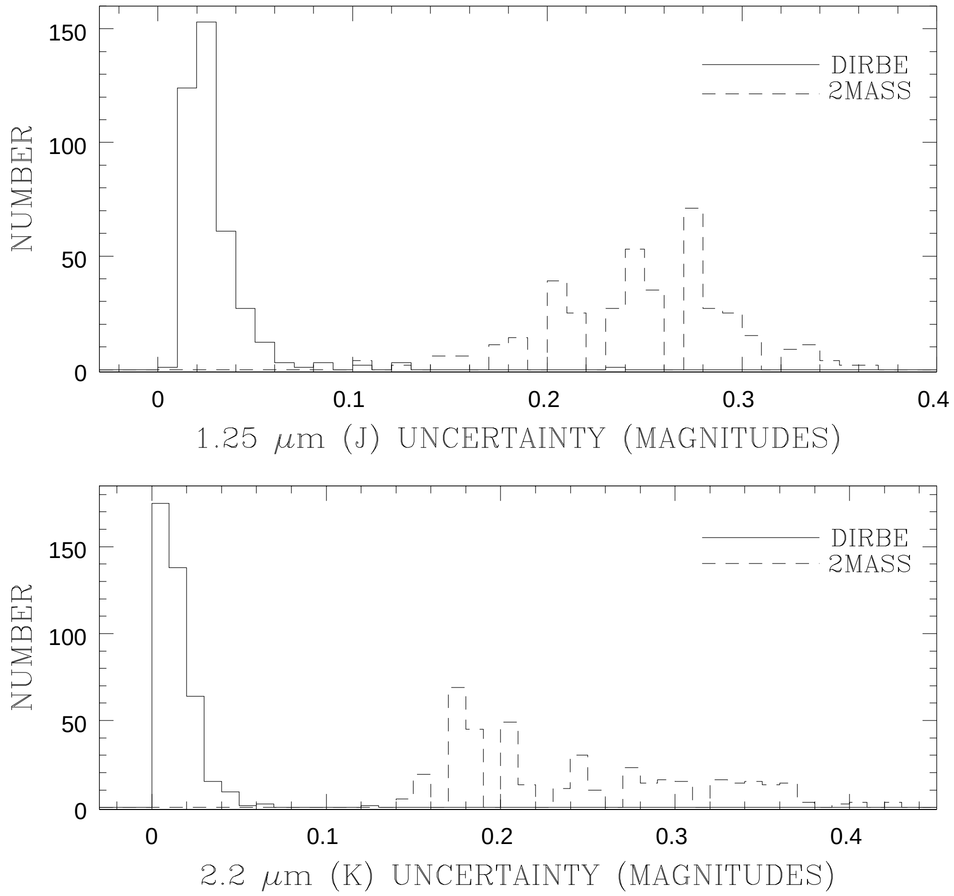

Fig. 7.— The distribution of uncertainties in the J (1.25 μm) and K (2.2 μm) magnitudes in DIRBE and 2MASS for the 791 brightest 2.2 μm sources in the sky (2MASS K $\leq$ 1.0 ($F_{2.2} \geq$ 266 Jy)).

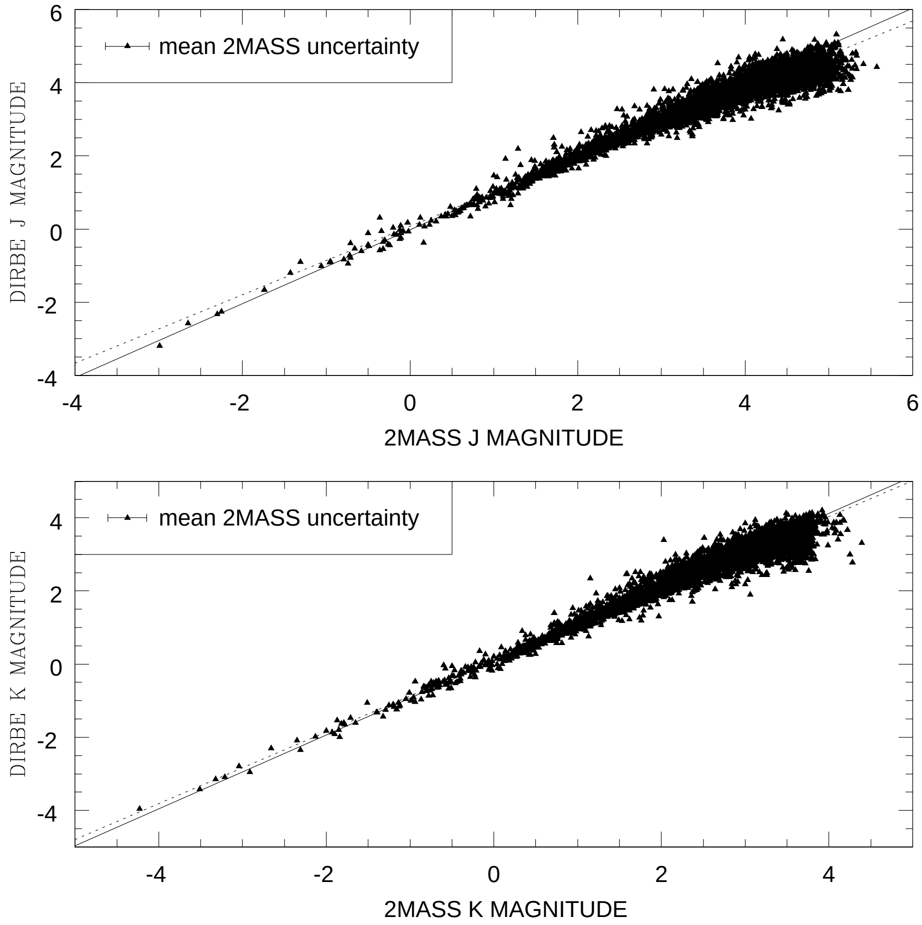

Fig. 8.— Top panel: A comparison of the 2MASS J magnitudes with those from DIRBE for the unflagged $|b| \geq 5°$ sources. Bottom panel: The 2MASS K magnitudes plotted against those from DIRBE, for unflagged sources. For clarity, errorbars are not included in the plot. Instead, the mean 2MASS uncertainty is shown in the upper left. The mean DIRBE uncertainty is smaller than the size of the datapoints. The best-fit lines as given in the text are shown; the solid lines are the best-fit for the data with 2MASS $K < 1$, while the dotted lines are for the full Catalog. Sources brighter than $J \sim 4.5$ and $K \sim 3.5$ are saturated in 2MASS (Cutri et al. 2003).

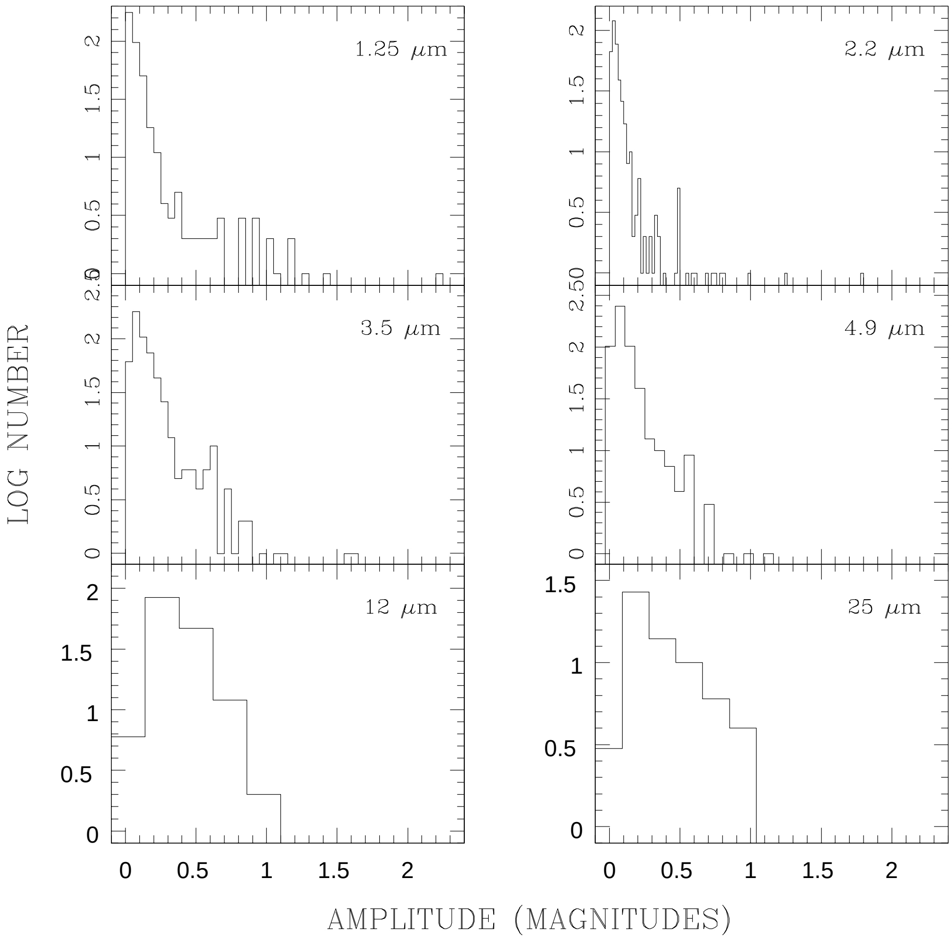

Fig. 9.— Histograms of the 1.25 μm $-$ 25 μm DIRBE amplitudes for the 791 sources with 2MASS K $\leq$ 1.0 ($F_{2.2}$ $\geq$ 266 Jy). This plot includes only unflagged sources, with filtered light curves containing $\geq$100 measurements. The bin sizes are set equal to the median uncertainties in the amplitude at each wavelength, which are 0.05, 0.02, 0.05, 0.07, 0.24, and 0.19 magnitudes at 1.25, 2.2, 3.5, 4.9, 12, and 25 μm, respectively.

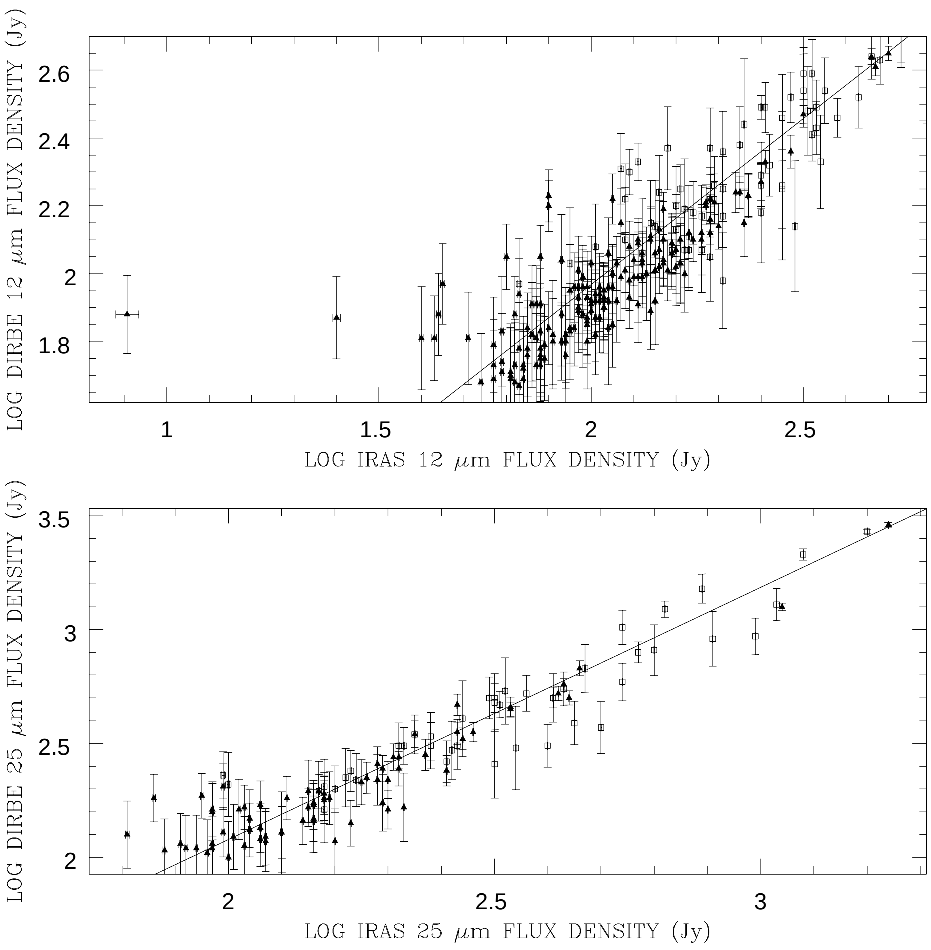

Fig. 10.— A comparison of the DIRBE 12 and 25 μm flux densities with those at IRAS, for unflagged $|b| \geq 5°$ sources. The best-fit lines as discussed in the text are shown. The very discrepant point to the left in the 12 μm plot is a nebula in the Large Magellanic Cloud, thus it may be extended or confused. The open squares are points with $\Delta(\mathrm{mag})/\sigma(\Delta(\mathrm{mag})) \geq 3$ in the DIRBE Catalog.

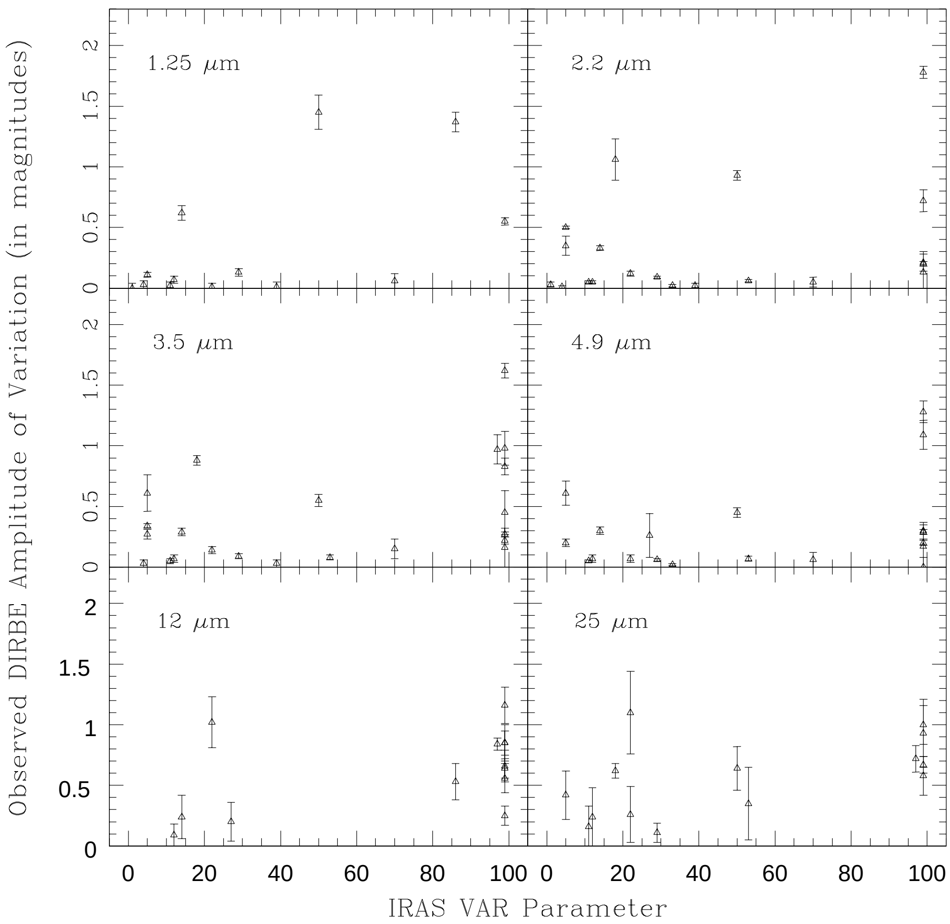

Fig. 11.— A comparison of the IRAS VAR parameter with the DIRBE amplitudes of variation at the six shortest DIRBE wavelengths, for the 207 brightest high Galactic latitude ($|b| \geq 5°$) 12 μm sources ($F_{12} \geq 150$ Jy). Sources that have been flagged in DIRBE or are low S/N ($\leq$5 at minimum) at a wavelength have been excluded at that wavelength. We also excluded sources flagged in IRAS as being possibly confused or in a region dominated by cirrus (IRAS CONFUSE flag $\neq 0$, CIRR1 > 3, or CIRR2 > 4). We have only included sources with high quality IRAS fluxes at both 12 and 25 μm (FQUAL12 and FQUAL25 = 3).

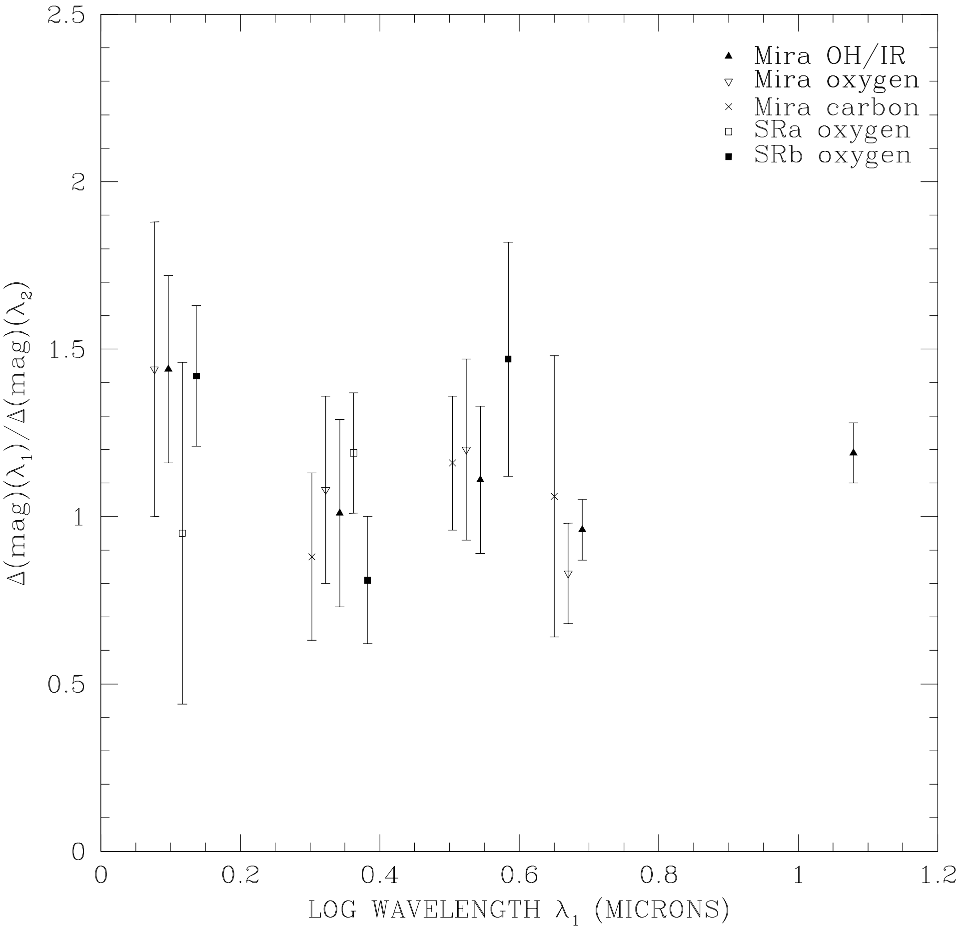

Fig. 12.— The ratio of the observed DIRBE amplitude at a given wavelength λ_1 to the amplitude at the next longest DIRBE wavelength λ_2, plotted as a function of λ_1. This plot excludes flagged stars and stars detected with less than S/N = 5 at minimum in the weekly-averaged light curves at both wavelengths. It also excludes stars with $\Delta(\mathrm{mag})/\sigma(\Delta(\mathrm{mag})) < 5$ at both wavelengths. Only classes of stars with at least 3 stars that fit these criteria at a given wavelength are plotted. For clarity, some datapoints have been shifted slightly in wavelength.

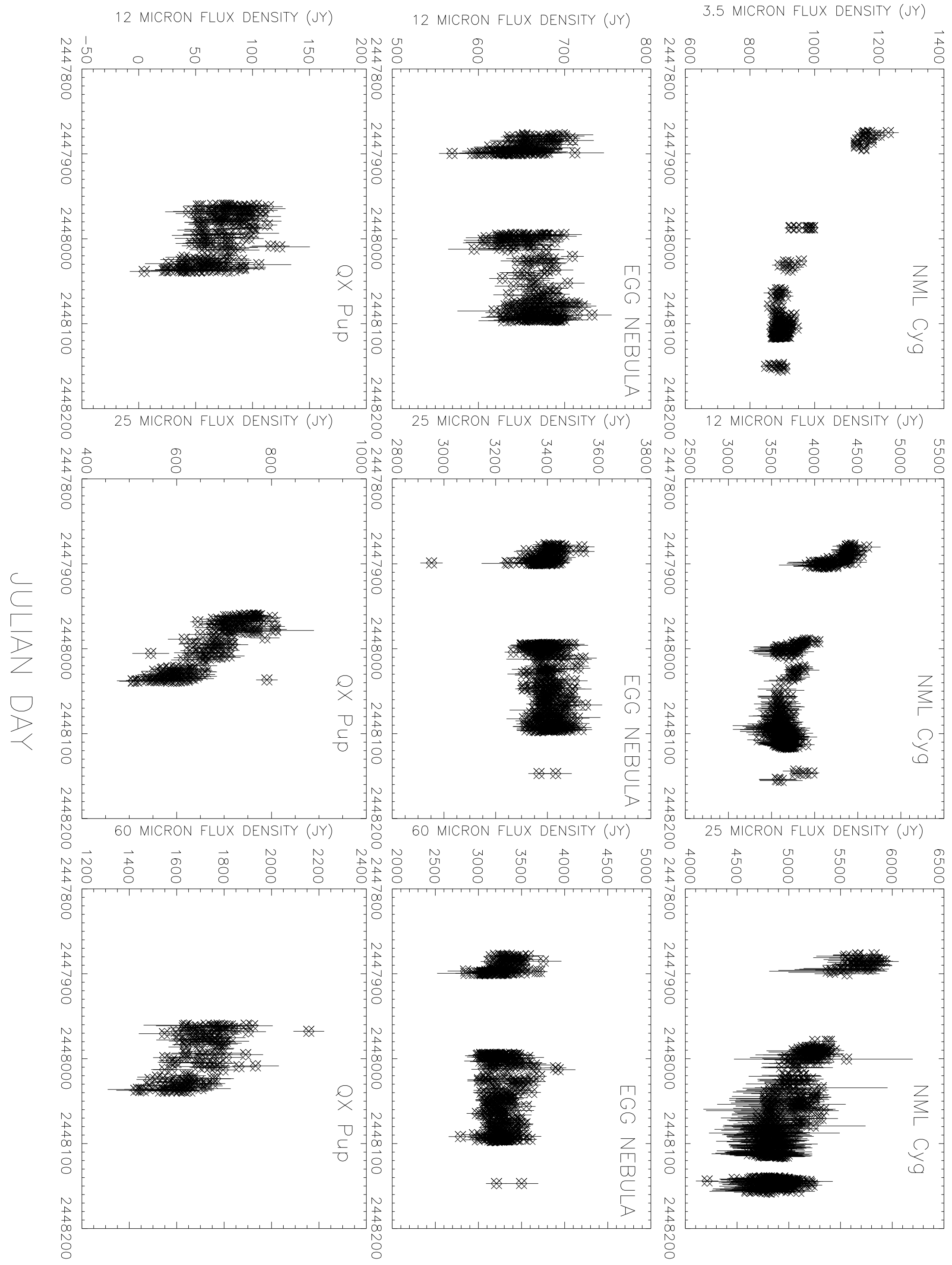

Fig. 13.— Some more example light curves. a) - c) DIRBE light curves at 3.5, 12, and 25 μm for NML Cyg. d) - f) DIRBE light curves at 12, 25, and 60 μm for the Egg Nebula (RAFGL 2688). g) - i) DIRBE light curves at 12, 25, and 60 μm for QX Pup (OH231.8+4.2).

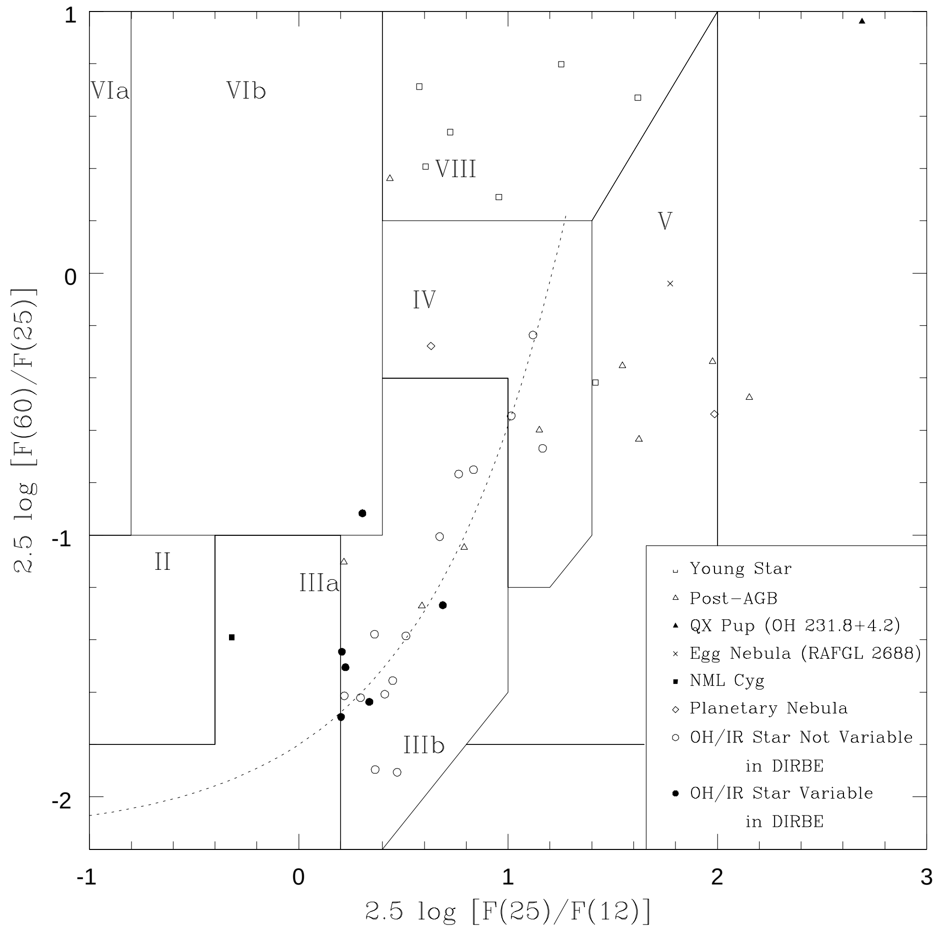

Fig. 14.— The IRAS color-color plot for the 43 unconfused objects in the DIRBE Catalog with a high S/N ($\geq$3) DIRBE light curve with at least 100 unfiltered data points at at least one wavelength, with IRAS $F_{25}/F_{12} \geq 1.2$ and $F_{60}/F_{100} \geq 2.5$, and with high quality IRAS Point Source Catalog fluxes at 12, 25, and 60 μm. Sources at all Galactic latitudes are included. Filled symbols represent objects which are variable in the DIRBE database; open symbols are objects that are not variable. The filled triangle in the upper right is QX Pup (OH 231.8+4.2). The cross marks the location based on the DIRBE data of the Egg Nebula (RAFGL 2688), a post-AGB object not variable in DIRBE, while the filled square shows the location of the supergiant NML Cyg, based on IRAS xscanpi results. The regions labeled with Roman numerals are from van der Veen & Habing (1988). The dashed line is the Bedijn (1987) evolutionary track for AGB stars.

Table 1. DIRBE PHOTOMETRY

NAME J2000 COORDINATES	2MASS NAME	IRAS/MSX NAME	1.25 μm						2.2 μm					
			F_ν (Jy)	σ (Jy)	<err> (Jy)	Δmag	$\sigma(\Delta$mag)	N	F_ν (Jy)	σ (Jy)	<err> (Jy)	Δmag	$\sigma(\Delta$mag)	N
D00000657P2553112	00000657+2553112	IRAS23575+2536	162.1	47.4	12.1	0.82	0.13	180	233.9	38.3	9.1	0.49	0.06	286
D00000690P2014145	00000690+2014145		47.8	6.9	6.2	0.35	0.22	341	55.0	6.5	5.5	0.30	0.16	404
D00001353P5541579	00001353+5541579		84.5	26.6	15.0	0.73	0.35	289	77.8	48.3	24.0	-99.90	-99.90	350
D00001815P6021016	00001815+6021016		324.8	52.1	25.0	0.22	0.13	265	462.0	68.2	32.3	0.29	0.12	332
D00010244P3830145	00010244+3830145	IRAS23584+3813	83.2	11.2	7.0	0.36	0.13	378	108.7	9.0	6.3	0.21	0.09	385

[a]NOTE:-Table 1 is presented in its entirety, including additional columns, in the electronic edition of the Astrophysical Journal Supplement. A portion is shown here for guidance regarding its form and content.

Table 2. CONFUSION FLAGS IN THE DIRBE POINT SOURCE CATALOG

FLAG	**DEFINITION**
1	If set to 1, there is another source within 0.5° of the target source above 25, 20, 20, 10, 30, 55, 320, and 765 Jy at 1.25, 2.2, 3.5, 4.9, 12, 25, 60, and 100 μm, respectively. This flag is not set at 140 and 240 μm.
2	If set to 1, the DIRBE photometry at minimum (in the weekly-averaged light curve) is greater than that of 2MASS or IRAS/MSX by more than 3σ, or the DIRBE photometry at maximum is less than that of 2MASS or IRAS/MSX by more than 3σ. This flag is not set at 3.5, 4.9, 140, and 240 μm.
3	If set to 1, the rms/<errorbar> for a 2-week period is greater than 3, suggesting confusion from an unknown source that is not completely corrected by filtering.

Table 3. STATISTICS ON THE DIRBE POINT SOURCE CATALOG: FULL SAMPLE

	1.25 μm	2.2 μm	3.5 μm	4.9 μm	12 μm	25 μm	60 μm	100 μm	140 μm	240 μm
Average Uncertainty per Datapoint in Raw Light Curves	33 Jy	38 Jy	27 Jy	21 Jy	107 Jy	256 Jy	1567 Jy	3207 Jy	8100 Jy	4510 Jy
Average Uncertainty per Datapoint in Filtered Light Curves	30 Jy	7 Jy	17 Jy	7 Jy	18 Jy	32 Jy	118 Jy	468 Jy	8100 Jy	4510 Jy
Estimated Completeness Limit for $\|b\| \geq 5^\circ$ for DIRBE Catalog Input List	90 Jy	60 Jy	60 Jy	50 Jy	90 Jy	165 Jy	–	–	–	–
Number Detected with S/N > 3 per Datapoint	6328	8203	6338	4688	894	502	448	395	136	209
Number Flagged for Companion in Beam	5943	9825	1126	4848	3907	3262	2513	2674	–	–
Number Flagged for Discrepancy with Other Photometry	198	152	–	–	308	173	249	186	–	–
Number Flagged for 2-week rms/<error> $\geq$ 3	1171	1997	7274	1989	2242	2325	3889	3940	2774	3322
Number Unflagged $>3\sigma$ Detections per Datapoint with N $\geq$ 100	2521	3361	3513	2352	311	145	56	77	44	47
Number Unflagged $>3\sigma$ Detections per Datapoint with $>3\sigma$ Amplitudes and N $\geq$ 100	126	223	310	222	85	42	0	2	1	0

Table 4. 2MASS/IRAS/MSX PHOTOMETRY FOR DIRBE CATALOG SOURCES

DIRBE name	TWOMASS name	IRAS name	2MASS PHOTOMETRY						IRAS PHOTOMETRY			
			J (mag)	σ_J (mag)	H (mag)	σ_H (mag)	K (mag)	σ_K (mag)	F_{12} (Jy)	F_{25} (Jy)	F_{60} (Jy)	F_{100} (Jy)
D00000657P2553112	00000657+2553112	IRAS23575+2536	2.225	0.296	1.317	0.158	0.915	0.188	53.780	22.560	3.330	1.783
D00000690P2014145	00000690+2014145		4.026	0.228	3.079	0.206	2.562	0.276	-99.990	-99.990	-99.990	-99.990
D00001353P5541579	00001353+5541579		4.490	0.292	3.479	0.216	2.987	0.288	-99.990	-99.990	-99.990	-99.990
D00001815P6021016	00001815+6021016		3.557	0.258	2.640	0.204	2.182	0.240	-99.990	-99.990	-99.990	-99.990
D00010244P3830145	00010244+3830145	IRAS23584+3813	3.542	0.248	2.630	0.178	2.083	0.234	19.770	8.800	1.410	1.011

[a] NOTE:-Table 3 is presented in its entirety, including additional columns with IRAS flags and VAR parameter, in the electronic edition of the Astrophysical Journal Supplement. A portion is shown here for guidance regarding its form and content.

Table 5. COMPANION INFORMATION

DIRBE NAME	WAVELENGTH (μm)	COMPANION NAME	F_ν (Jy)	OFFSET (degrees)
D00001353P5541579	1.25	2MASS00032146+5540518	124.1	0.441882
D00001353P5541579	2.20	2MASS00032146+5540518	234.4	0.441882
D00001353P5541579	3.50	AFGL 5	199.2	0.435020
D00001353P5541579	4.90	AFGL 5	186.4	0.435020
D00001353P5541579	4.90	RAFGL 5	155.0	0.435020
D00001353P5541579	12.00	IRAS00007+5524	97.6	0.441621

[a]NOTE:-Table 4 is presented in its entirety in the electronic edition of the Astronomical Journal. A portion is shown here for guidance regarding its form and content.

Table 6. INCOMPLETENESS OF DIRBE CATALOG DUE TO CONFUSION

	1.25 μm	2.2 μm	12 μm	25 μm	60 μm	100 μm
Nominal Completeness Limits (Jy)	90	60	90	165	960	2295
Number in IRAS/2MASS/MSX > DIRBE 3σ limit	2511	5389	727	485	461	454
Number of these with all points removed by filtering	685	1211	163	262	336	392
Percent with all removed by filtering	27	22	22	54	72	86

Table 7. STATISTICS ON CATALOG SUBSET WITH 2MASS K < 1.0

	1.25 μm	2.2 μm	3.5 μm	4.9 μm	12 μm	25 μm	60 μm	100 μm	140 μm	240 μm
Number Detected with S/N $>$ 3	462	570	765	699	279	98	14	14	1	2
Number Flagged for Companion in Beam	153	252	20	138	120	52	22	18	0	0
Number Flagged for Discrepancy with Other Photometry	4	1	0	0	63	18	7	12	0	0
Number Flagged for 2-week rms/<error> $\geq$ 3	45	92	213	98	106	89	139	165	62	63
Number Unflagged $\geq 3\sigma$ Detections with N $\geq$ 100	215	271	540	435	149	52	5	1	1	1
Number Unflagged $>3\sigma$ Detections with $>3\sigma$ Amplitudes and N $\geq$ 100	57	90	123	77	20	11	0	0	0	0

Table 8. DIRBE CATALOG ASSOCIATIONS AND OTHER INFORMATION

DIRBE NAME	TWOMASS NAME	IRAS NAME	FIRST SIMBAD NAME	SIMBAD OBJECT TYPE	SIMBAD SPECTRAL TYPE	SIMBAD OFFSET ($''$)	SECOND SIMBAD NAME
D00000657P2553112	00000657+2553112	IRAS23575+2536	V* Z Peg	Mi*	M7e	0.2	
D00000690P2014145	00000690+2014145		V* EP Peg	sr*	M ...	0.1	IRAS 23575+1957
D00001353P5541579	00001353+5541579		HD 224719	*	M ...	0.1	
D00001815P6021016	00001815+6021016		HD 224754	*	M2	0.1	
D00010244P3830145	00010244+3830145	IRAS23584+3813	DO 22623	*	M0	5.4	

[a]NOTE:-Table 7 is presented in its entirety, including additional columns with more SIMBAD data, GCVS/NSV/NSV information, IRAS spectral types, and OH/IR star identifications, in the electronic edition of the Astrophysical Journal Supplement. A portion is shown here for guidance regarding its form and content.

Table 9. STATISTICS ON ASSOCIATIONS: FULL CATALOG

Type		1.25 μm	2.2 μm	3.5 μm	4.9 μm	12 μm	25 μm	60 μm	100 μm	140 μm	240 μm
M Mira/SRa/SRb/Lb	S/N $\geq$ 3 per datapoint	1353	1802	1732	1433	249	98	18	20	1	1
	unflagged with N $\geq$ 100	612	836	1157	875	132	51	5	3	1	1
	$\geq 3\sigma$ amplitude	94	160	191	127	30	17	0	0	0	0
	percent variable	15	19	17	15	23	33	0	0	0	0
M other/unspecified	S/N $\geq$ 3 per datapoint	1394	1905	1468	1031	113	54	41	51	8	7
	unflagged with N $\geq$ 100	517	755	834	524	41	14	5	12	2	2
	$\geq 3\sigma$ amplitude	6	13	29	13	10	3	0	1	0	0
	percent variable	1	2	3	2	24	21	0	8	0	0
K Mira/SRa/SRb/Lb	S/N $\geq$ 3 per datapoint	57	77	38	25	2	3	1	1	0	0
	unflagged with N $\geq$ 100	28	38	22	16	0	2	0	0	0	0
	$\geq 3\sigma$ amplitude	1	1	1	0	0	0	0	0	0	0
	percent variable	4	3	5	0	–	0	–	–	–	–
K other/unspecified	S/N $\geq$ 3 per datapoint	2054	2394	1335	746	73	37	37	51	5	5
	unflagged with N $\geq$ 100	851	1066	741	384	18	7	12	21	0	1
	$\geq 3\sigma$ amplitude	1	1	1	0	0	0	0	0	0	0
	percent variable	0	0	0	0	0	0	0	0	–	0
S Mira/SRa/SRb/Lb	S/N $\geq$ 3 per datapoint	26	40	45	34	6	5	0	0	0	0
	unflagged with N $\geq$ 100	6	11	30	13	1	2	0	0	0	0
	$\geq 3\sigma$ amplitude	3	6	12	2	1	1	0	0	0	0
	percent variable	50	55	40	15	100	50	–	–	–	–
S other/unspecified	S/N $\geq$ 3 per datapoint	3	4	7	7	4	0	3	1	0	0
	unflagged with N $\geq$ 100	1	1	3	2	0	0	0	0	0	0
	$\geq 3\sigma$ amplitude	0	0	0	0	0	0	0	0	0	0
	percent variable	0	0	0	0	–	–	–	–	–	–
C Mira/SRa/SRb/Lb	S/N $\geq$ 3 per datapoint	74	130	187	163	58	15	4	2	0	0
	unflagged with N $\geq$ 100	23	41	110	80	33	9	1	0	0	0
	$\geq 3\sigma$ amplitude	10	21	32	23	12	3	0	0	0	0
	percent variable	43	51	29	29	36	33	0	0	–	–
C other/unspecified	S/N $\geq$ 3 per datapoint	28	61	86	124	41	19	7	9	0	0
	unflagged with N $\geq$ 100	5	8	40	54	23	8	1	2	0	0
	$\geq 3\sigma$ amplitude	1	2	15	30	11	5	0	0	0	0
	percent variable	20	25	38	56	48	62	0	0	–	–
Star Formation	S/N $\geq$ 3 per datapoint	6	17	51	47	49	48	53	49	19	30
	unflagged with N $\geq$ 100	0	2	10	9	4	6	5	4	6	6
	$\geq 3\sigma$ amplitude	0	0	0	0	0	0	0	0	1	0
	percent variable	–	0	0	0	0	0	0	0	17	0
post-AGB	S/N $\geq$ 3 per datapoint	1	3	4	8	4	10	5	2	0	0
	unflagged with N $\geq$ 100	0	0	0	0	0	0	0	0	0	0
	$\geq 3\sigma$ amplitude	0	0	0	0	0	0	0	0	0	0
	percent variable	–	–	–	–	–	–	–	–	–	–
Planetary Nebulae	S/N $\geq$ 3 per datapoint	1	1	3	4	3	7	2	2	0	0
	unflagged with N $\geq$ 100	0	0	1	2	2	4	1	1	0	0
	$\geq 3\sigma$ amplitude	0	0	0	0	0	0	0	0	0	0
	percent variable	–	–	0	0	0	0	0	0	–	–

Table 9—Continued

Type		1.25 μm	2.2 μm	3.5 μm	4.9 μm	12 μm	25 μm	60 μm	100 μm	140 μm	240 μm
Galaxies	S/N $\geq$ 3 per datapoint	1	0	0	0	1	2	2	2	0	0
	unflagged with N $\geq$ 100	1	0	0	0	0	1	0	0	0	0
	$\geq 3\sigma$ amplitude	0	0	0	0	0	0	0	0	0	0
	percent variable	0	0	0	0	0	0	0	0	0	0
O Other/Unspecified	S/N $\geq$ 3 per datapoint	3	3	3	2	1	1	4	3	1	2
	unflagged with N $\geq$ 100	1	0	0	0	0	0	2	2	0	0
	$\geq 3\sigma$ amplitude	0	0	0	0	0	0	0	0	0	0
	percent variable	0	–	–	–	–	–	0	0	–	–
B Other/Unspecified	S/N $\geq$ 3 per datapoint	64	62	37	32	9	12	17	15	3	3
	unflagged with N $\geq$ 100	29	15	17	14	2	1	4	2	0	0
	$\geq 3\sigma$ amplitude	0	0	0	0	0	0	0	0	0	0
	percent variable	0	0	0	0	0	0	0	0	–	–
A Other/Unspecified	S/N $\geq$ 3 per datapoint	131	100	62	43	9	6	5	3	1	1
	unflagged with N $\geq$ 100	53	42	39	20	5	1	0	1	0	0
	$\geq 3\sigma$ amplitude	0	0	0	0	0	0	0	0	0	0
	percent variable	0	0	0	0	0	0	–	0	–	–
F Other/Unspecified	S/N $\geq$ 3 per datapoint	147	133	67	45	6	0	5	5	1	1
	unflagged with N $\geq$ 100	62	60	39	22	1	0	0	1	0	0
	$\geq 3\sigma$ amplitude	0	0	0	0	0	0	0	0	0	0
	percent variable	0	0	0	0	0	–	–	0	–	–
G Other/Unspecified	S/N $\geq$ 3 per datapoint	388	408	239	149	3	1	1	1	0	0
	unflagged with N $\geq$ 100	179	182	140	94	0	0	0	1	0	0
	$\geq 3\sigma$ amplitude	1	0	0	0	0	0	0	0	0	0
	percent variable	1	0	0	0	–	–	–	0	–	–
Other/Unspecified	S/N $\geq$ 3 per datapoint	599	1066	977	798	264	186	244	180	97	159
	unflagged with N $\geq$ 100	153	304	330	243	46	35	19	28	35	37
	$\geq 3\sigma$ amplitude	9	19	29	27	21	13	0	1	0	0
	percent variable	6	6	9	11	46	37	0	4	0	0
Total	S/N $\geq$ 3 per datapoint	6328	8203	6338	4688	894	502	448	395	136	209
	unflagged with N $\geq$ 100	2521	3361	3513	2352	311	145	56	77	44	47
	$\geq 3\sigma$ amplitude	126	223	310	222	85	42	0	2	1	0
	percent variable	5	7	9	9	27	29	0	3	2	0

Table 10. STATISTICS ON ASSOCIATIONS: 2MASS K < 1.0 SUBSAMPLE

Type		1.25 μm	2.2 μm	3.5 μm	4.9 μm	12 μm	25 μm	60 μm	100 μm	140 μm	240 μm
M Mira/SRa/SRb/Lb	S/N $\geq$ 3 per datapoint	266	316	417	387	173	62	8	8	0	0
	unflagged with N $\geq$ 100	129	161	302	251	98	34	4	1	0	0
	$\geq 3\sigma$ amplitude	41	69	91	61	11	6	0	0	0	0
	percent variable	32	43	30	24	11	18	0	0	–	–
M other/unspecified	S/N $\geq$ 3 per datapoint	76	98	138	121	39	17	4	2	1	1
	unflagged with N $\geq$ 100	35	42	93	72	15	7	1	0	1	1
	$\geq 3\sigma$ amplitude	3	7	11	4	1	1	0	0	0	0
	percent variable	9	17	12	6	7	14	0	–	0	0
K Mira/SRa/SRb/Lb	S/N $\geq$ 3 per datapoint	4	5	7	7	2	2	0	0	0	0
	unflagged with N $\geq$ 100	2	2	5	4	0	2	0	0	0	0
	$\geq 3\sigma$ amplitude	1	0	1	0	0	0	0	0	0	0
	percent variable	50	0	20	0	–	0	–	–	–	–
K other/unspecified	S/N $\geq$ 3 per datapoint	61	79	103	92	18	2	1	1	0	0
	unflagged with N $\geq$ 100	28	40	68	56	11	0	0	0	0	0
	$\geq 3\sigma$ amplitude	0	0	0	0	0	0	0	0	0	0
	percent variable	0	0	0	0	0	–	–	–	–	–
S Mira/SRa/SRb/Lb	S/N $\geq$ 3 per datapoint	3	3	9	6	5	4	0	0	0	0
	unflagged with N $\geq$ 100	1	2	5	2	1	2	0	0	0	0
	$\geq 3\sigma$ amplitude	1	2	3	1	1	1	0	0	0	0
	percent variable	100	100	60	50	100	50	–	–	–	–
C Mira/SRa/SRb/Lb	S/N $\geq$ 3 per datapoint	32	37	49	47	30	5	1	1	0	0
	unflagged with N $\geq$ 100	14	14	36	28	18	2	0	0	0	0
	$\geq 3\sigma$ amplitude	10	11	12	9	3	0	0	0	0	0
	percent variable	71	79	33	32	17	0	–	–	–	–
B Other/Unspecified	S/N $\geq$ 3 per datapoint	1	2	2	2	0	0	0	0	0	0
	unflagged with N $\geq$ 100	1	1	1	1	0	0	0	0	0	0
	$\geq 3\sigma$ amplitude	0	0	0	0	0	0	0	0	0	0
	percent variable	0	0	0	0	–	–	–	–	–	–
A Other/Unspecified	S/N $\geq$ 3 per datapoint	2	5	7	7	2	0	0	0	0	0
	unflagged with N $\geq$ 100	1	1	6	2	1	0	0	0	0	0
	$\geq 3\sigma$ amplitude	0	0	0	0	0	0	0	0	0	0
	percent variable	0	0	0	0	0	–	–	–	–	–
F Other/Unspecified	S/N $\geq$ 3 per datapoint	3	4	6	6	2	0	0	0	0	0
	unflagged with N $\geq$ 100	1	1	6	4	1	0	0	0	0	0
	$\geq 3\sigma$ amplitude	0	0	0	0	0	0	0	0	0	0
	percent variable	0	0	0	0	0	–	–	–	–	–
G Other/Unspecified	S/N $\geq$ 3 per datapoint	9	12	15	13	1	0	0	0	0	0
	unflagged with N $\geq$ 100	2	5	9	9	0	0	0	0	0	0
	$\geq 3\sigma$ amplitude	0	0	0	0	0	0	0	0	0	0
	percent variable	0	0	0	0	–	–	–	–	–	–
Other/Unspecified	S/N $\geq$ 3 per datapoint	5	9	12	11	7	6	0	0	0	1
	unflagged with N $\geq$ 100	1	2	9	6	4	5	0	0	0	0
	$\geq 3\sigma$ amplitude	1	1	5	2	4	3	0	0	0	0
	percent variable	100	50	56	33	100	60	–	–	–	–

Table 10—Continued

Type		1.25 μm	2.2 μm	3.5 μm	4.9 μm	12 μm	25 μm	60 μm	100 μm	140 μm	240 μm
Total	S/N $\geq$ 3 per datapoint	462	570	765	699	279	98	14	12	1	2
	unflagged with N $\geq$ 100	215	271	540	435	149	52	5	1	1	1
	$\geq 3\sigma$ amplitude	57	90	123	77	20	11	0	0	0	0
	percent variable	27	33	23	18	13	21	0	0	0	0

Table 11. BRIGHTEST 1.25 μm SOURCES IN DIRBE CATALOG

DIRBE NAME	2MASS NAME	IRAS NAME	1.25 μm F_ν	σ	$<err>$	Δmag	$\sigma(\Delta$mag)	N	Flags[a]	SIMBAD NAME	SPECTRAL TYPE	VAR TYPE
D05551028P0724255	05551028+0724255	05524+0723	30122	922	510	0.08	0.03	99	000	α Ori	M1	SR
D04364544M6204379	04364544-6204379	04361-6210	16977	642	386	0.02	0.04	26	000	R Dor	M8III	SR
D17143885P1423253	17143885+1423253	17123+1426	13590	362	388	0.02	0.04	26	000	α Her	M5Ib-II	SR
D14153968P1910558	14153968+1910558	14133+1925	12763	247	248	0.04	0.03	229	000	α Boo	K1.5III	
D22424003M4653044	22424003-4653044	22396-4708	11397	398	234	0.06	0.03	123	001	β Gru	M5III	
D13490199M2822034	13490199-2822034	13462-2807	7331	1753	123	0.11	0.02	29	000	W Hya	M7e	SR
D05164138P4559525	05164138+4559525	05130+4556	5451	72	105	0.01	0.03	61	000	α Aur	G5IIIe+...	
D23034644P2804580	13490199-2822034	13462-2807	4781	109	93	0.05	0.03	297	000	β Peg	M2.5II-III	
D09473348P1125436	09473348+1125436	09448+1139	4421	835	86	0.37	0.03	50	101	R Leo	M8IIIe	M
D07133229M4438233	07133229-4438233	07120-4433	4019	269	113	0.17	0.04	102	000	L_2 Pup	M5IIIe	SR

[a] If the first confusion flag is set to 1, there is another source in the DIRBE beam with a 2MASS J band flux density above 25 Jy. If the second confusion flag is set to 1, the DIRBE photometry at minimum (in the weekly-averaged light curve) is greater than that of 2MASS by more than 3σ, or the DIRBE photometry at maximum is less than that of 2MASS by more than 3σ. If this flag is set, this may mean a second source in the beam, extended emission, or large variations not observed in DIRBE. If the third flag is set, the rms/<errorbar> for a 2-week period is greater than 3, suggesting confusion from an unknown source that is not completely corrected by filtering.

Table 12. BRIGHTEST 2.2 μm SOURCES IN DIRBE CATALOG

DIRBE	2MASS	IRAS				2.2 μm				SIMBAD	SPECTRAL	VAR
NAME	NAME	NAME	F_ν	σ	$<err>$	Δmag	$\sigma(\Delta$mag$)$	N	Flags[a]	NAME	TYPE	TYPE
D05551028P0724255	05551028+0724255	05524+0723	29995	889	210	0.07	0.01	72	100	α Ori	M1	SR
D04364544M6204379	04364544-6204379	04361-6210	25601	1898	163	0.19	0.01	119	000	R Dor	M8IIIe	SR
D16292443M2625549	16292443-2625549	16262-2619A	23270	179	143	0.01	0.01	44	100	α Sco	M1.5Ib	SR
D17143885P1423253	17143885+1423253	17123+1426	15614	229	107	0.04	0.01	193	000	α Her	M5II	SR
D22424003M4653044	22424003-4653044	22396-4708	12123	107	78	0.02	0.01	190	000	β Gru	M5III	
D12310993M5706474	12310993-5706474	12283-5650	11710	82	97	0.00	0.01	35	100	γ Cru	M3.5III	
D13490199M2822034	13490199-2822034	13462-2807	11442	2506	85	0.50	0.01	160	000	W Hya	M7e	SR
D14153968P1910558	14153968+1910558	14133+1925	10073	61	62	0.01	0.01	299	000	α Boo	K1.5III	
D04355524P1630331	04355524+1630331	04330+1624	8739	42	49	0.00	0.01	40	000	α Tau	K5III	
D09473348P1125436	09473348+1125436	09448+1139	7680	976	52	0.26	0.01	70	101	R Leo	M8IIIe	M

[a]If the first confusion flag is set to 1, there is another source in the DIRBE beam with a 2MASS K band flux density above 20 Jy. If the second confusion flag is set to 1, the DIRBE photometry at minimum in the weekly-averaged light curve is greater than that of 2MASS by more than 3σ, or the DIRBE photometry at maximum is less than that of 2MASS by more than 3σ. If this flag is set, this may mean a second source in the beam, extended emission, or large variations not observed in DIRBE. If the third flag is set, the rms/<errorbar> for a 2-week period is greater than 3, suggesting confusion from an unknown source that is not completely corrected by filtering.

Table 13. BRIGHTEST 3.5 μm SOURCES IN DIRBE CATALOG

DIRBE	2MASS	IRAS	3.5 μm							SIMBAD	SPECTRAL	VAR
NAME	NAME	NAME	F_ν	σ	$<err>$	Δmag	$\sigma(\Delta$mag$)$	N	Flags[a]	NAME	TYPE	TYPE
D05551028P0724255	05551028+0724255	05524+0723	17065	546	228	0.08	0.02	312	000	α Ori	M1	SR
D04364544M6204379	04364544-6204379	04361-6210	15611	955	233	0.21	0.02	684	000	R Dor	M8IIIe	SR
D16292443M2625549	16292443-2625549	16262-2619A	13063	233	188	0.05	0.02	274	000	α Sco	M1.5Ib	SR
D17143885P1423253	17143885+1423253	17123+1426	8310	160	122	0.06	0.02	475	000	α Her	M5II	SR
D13490199M2822034	13490199-2822034	13462-2807	7945	1107	105	0.34	0.02	366	000	W Hya	M7e	SR
D22424003M4653044	22424003-4653044	22396-4708	6248	124	89	0.04	0.02	317	001	β Gru	M5III	
D12310993M5706474	12310993-5706474	12283-5650	5920	90	89	0.03	0.02	803	000	γ Cru	M3.5III	
D09473348P1125436	09473348+1125436	09448+1139	5104	589	72	0.33	0.02	179	000	R Leo	M8IIIe	M
D14153968P1910558	14153968+1910558	14133+1925	4868	73	73	0.04	0.02	549	000	α Boo	K1.5III	
D04355524P1630331	04355524+1630331	04330+1624	4339	70	68	0.02	0.02	354	000	α Tau	K5III	

[a]If the first confusion flag is set to 1, there is another source in the DIRBE beam with a 3.5 μm flux density above 20 Jy in the Catalog of Infrared Observations. The second confusion flag is not set at 3.5 μm. If the third flag is set, the rms/<errorbar> for a 2-week period is greater than 3, suggesting confusion from an unknown source that is not completely corrected by filtering.

Table 14. BRIGHTEST 4.9 μm SOURCES IN DIRBE CATALOG

DIRBE	2MASS	IRAS	4.9 μm							SIMBAD	SPECTRAL	VAR
NAME	NAME	NAME	F_ν	σ	$<err>$	Δmag	$\sigma(\Delta$mag$)$	N	Flags[a]	NAME	TYPE	TYPE
D09475740P1316435	09475740+1316435	09452+1330	9011	5742	61	1.37	0.01	89	001	CW Leo	C	Mira
D04364544M6204379	04364544-6204379	04361-6210	8729	256	41	0.11	0.01	530	000	R Dor	M8IIIe	SR
D05551028P0724255	05551028+0724255	05524+0723	7142	326	31	0.11	0.01	67	000	α Ori	M1	SR
D16292443M2625549	16292443-2625549	16262-2619A	5650	31	25	0.01	0.01	71	100	α Sco	M1Ib+	SR
D13490199M2822034	13490199-2822034	13462-2807	5378	326	25	0.18	0.01	297	001	W Hya	M7e	M
D17143885P1423253	17143885+1423253	17123+1426	3616	54	17	0.04	0.01	135	100	α Her	M5II	SR
D09473348P1125436	09473348+1125436	09448+1139	3459	364	17	0.28	0.01	91	101	R Leo	M8IIIe	M
D02192081M0258393	02192081-0258393	02168-0312	3221	812	17	0.70	0.01	148	001	omi Cet	M7IIIe	M
D22424003M4653044	22424003-4653044	22396-4708	2684	17	14	0.02	0.01	294	000	β Gru	M5III	
D07133229M4438233	07133229-4438233	07120-4433	2644	67	14	0.12	0.01	1278	001	L_2 Pup	M5IIIe	SR

[a]If the first confusion flag is set to 1, there is another source in the DIRBE beam with a 4.9 μm flux density above 10 Jy in the Catalog of Infrared Observations or in the Egan & Price (1996) synthetic 4.2 μm catalog. The second confusion flag is not set at 4.9 μm. If the third flag is set, the rms/<errorbar> for a 2-week period is greater than 3, suggesting confusion from an unknown source that is not completely corrected by filtering.

Table 15. BRIGHTEST 12 μm SOURCES IN DIRBE CATALOG

DIRBE NAME	2MASS NAME	IRAS NAME	12 μm F_ν	σ	$<err>$	Δmag	$\sigma(\Delta$mag$)$	N	Flags[a]	SIMBAD NAME	SPECTRAL TYPE	VAR TYPE
D09475740P1316435	09475740+1316435	09452+1330	31773	7661	356	0.33	0.02	51	110	CW Leo	C	M
D05351646M0523230	05351646-0523230		19690	491	266	0.03	0.02	59	100	θ Ori C	O6pe	
D05353020M0515490		05330-0517	19114	1205	254	0.08	0.02	74	111			
D05351000M0527470		05327-0529	18596	1321	284	0.05	0.02	48	110	LP Ori	B1.5Vp	Orion
D05353430M0514520		05331-0515	17565	2292	253	0.09	0.02	35	111			
D11142900M6118000		11123-6101	9518	847	166	0.16	0.03	82	111	OH CSI-61-11124	WR	
D07225830M2546030	07225830-2546030	07209-2540	9278	299	88	0.07	0.01	66	110	VY CMa	M3/M4II:	
D11155060M6113420		11136-6056	8676	516	136	0.10	0.02	78	111			
D08590440M4730370		08573-4718	5378	201	84	0.02	0.02	89	111	Maser 267.94-01.06		
D05413870M0151190		05391-0152	4897	261	82	0.08	0.03	93	111	NGC 2024	cluster	

[a]If the first confusion flag is set to 1, there is another source in the DIRBE beam with an IRAS 12 μm flux density above 30 Jy. If the second confusion flag is set to 1, the DIRBE photometry at minimum is greater than that of IRAS by more than 3σ, or the DIRBE photometry at maximum is less than that of IRAS by more than 3σ. If this flag is set, this may mean a second source in the beam, extended emission, or large variations not observed in DIRBE. If the third flag is set, the rms/<errorbar> for a 2-week period is greater than 3, suggesting confusion from an unknown source that is not completely corrected by filtering.

Table 16. BRIGHTEST 25 μm SOURCES IN DIRBE CATALOG

DIRBE NAME	2MASS NAME	IRAS NAME	25 μm F_ν	σ	$<err>$	Δmag	$\sigma(\Delta\mathrm{mag})$	N	Flags[a]	SIMBAD NAME	SPECTRAL TYPE	VAR TYPE
D08590440M4730370		08573-4718	28682	951	200	0.00	0.01	24	111	Maser 267.94-01.06		
D09475740P1316435	09475740+1316435	09452+1330	28611	4508	230	0.18	0.01	47	110	CW Leo	C	M
D10463100M6003470		10445-5947	17092	3716.	642	0.01	0.06	23	110			
D07225830M2546030	07225830-2546030	07209-2540	12346	345	96.	0.10	0.01	397	110	VY CMa	M3/M4II:	
D18172538M1145416	18172538-1145416	18146-1146	10368	2143	677	0.06	0.10	26	110			
D10482740M5951210		10464-5935	8540	4059	829	0.28	0.16	32	110			
D20343600P4105541	20343600+4105541		6394	591	806	0.04	0.21	36	100	HD 196241	K5	
D18312470M0205320		18288-0207	6162	229	79	0.03	0.02	46	111	W40		
D20350950P4113180		20333+4102	6062	581	883	0.12	0.23	74	110	G080.4+00.4		
D20381718P4204251	20381718+4204251		5962	1065	1090	0.27	0.29	101	000	HD 196819	K2.5IIb	

[a]If the first confusion flag is set to 1, there is another source in the DIRBE beam with an IRAS 25 μm flux density above 55 Jy. If the second confusion flag is set to 1, the DIRBE photometry at minimum is greater than that of IRAS by more than 3σ, or the DIRBE photometry at maximum is less than that of IRAS by more than 3σ. If this flag is set, this may mean a second source in the beam, extended emission, or large variations not observed in DIRBE. If the third flag is set, the rms/<errorbar> for a 2-week period is greater than 3, suggesting confusion from an unknown source that is not completely corrected by filtering.

Table 17. MEAN DIRBE AMPLITUDES OF VARIATION

Var	Spectral	1.25 μm			2.2 μm			3.5 μm			4.9 μm			12 μm			25 μm		
Type	Type	$<\Delta$mag$>$	$<\sigma>$	N	$<\Delta$mag$>$	$<\sigma>$	N	$<\Delta$mag$>$	$<\sigma>$	N	$<\Delta$mag$>$	$<\sigma>$	N	$<\Delta$mag$>$	$<\sigma>$	N	$<\Delta$mag$>$	$<\sigma>$	N
Mira	OH/IR	0.82±0.58	0.15	12	0.58±0.31	0.13	36	0.68±0.29	0.11	31	0.55±0.28	0.13	37	0.66±0.23	0.13	13	0.61±0.16	0.12	9
Mira	oxygen	0.53±0.33	0.11	93	0.45±0.25	0.12	160	0.50±0.23	0.12	152	0.37±0.21	0.13	174	0.60±0.27	0.15	26	0.64±0.22	0.18	12
Mira	carbon	0.56±0.26	0.18	4	0.64±0.42	0.12	17	0.77±0.35	0.11	20	0.45±0.35	0.10	38	0.59±0.18	0.14	18	0.52±0.19	0.14	7
Mira	S	0.46±0.27	0.13	3	0.34±0.23	0.14	7	0.67±0.23	0.11	9	0.38±0.19	0.14	9	0.92	0.10	1	0.88	0.23	1
SRa	OH/IR	–	0.13	0	0.74	0.24	1	–	0.11	0	–	0.14	0	0.61	0.09	1	0.70	0.22	1
SRa	oxygen	0.22±0.21	0.13	39	0.19±0.13	0.12	46	0.26±0.16	0.12	36	0.17±0.12	0.12	30	0.22±0.09	0.15	4	0.22	0.17	1
SRa	carbon	0.45±0.41	0.10	5	0.24±0.20	0.10	5	0.30±0.16	0.10	7	0.29±0.17	0.11	5	0.16	0.03	1	–	0.17	0
SRb	OH/IR	–	0.19	0	0.24	0.17	1	0.35	0.24	1	–	0.11	0	–	0.03	0	–	0.17	0
SRb	oxygen	0.12±0.10	0.11	345	0.12±0.10	0.09	380	0.18±0.10	0.11	333	0.15±0.08	0.13	264	0.24±0.09	0.19	24	0.22±0.07	0.17	10
SRb	carbon	0.16±0.15	0.10	20	0.11±0.10	0.06	19	0.17±0.09	0.08	27	0.15±0.11	0.10	27	0.27±0.07	0.21	7	–	0.17	0
SRb	S	0.16±0.06	0.11	3	0.13±0.14	0.10	5	0.23±0.16	0.11	6	0.25±0.28	0.12	3	–	0.21	0	0.10	0.09	1
SRc	OH/IR	–	0.11	0	–	0.10	0	0.23	0.14	1	0.27	0.08	1	0.38±0.18	0.16	2	0.47±0.26	0.21	2
SRc	oxygen	0.10±0.08	0.08	16	0.09±0.08	0.08	15	0.18±0.17	0.09	22	0.14±0.08	0.11	18	0.20±0.05	0.19	4	0.19±0.03	0.17	3
Lb	oxygen	0.12±0.10	0.12	393	0.12±0.10	0.11	436	0.20±0.12	0.13	322	0.17±0.11	0.14	260	0.26±0.03	0.21	6	0.20±0.06	0.20	2
Lb	carbon	0.19±0.18	0.11	14	0.15±0.22	0.11	24	0.26±0.21	0.12	26	0.28±0.32	0.12	24	0.50±0.23	0.17	2	0.69	0.24	1
Lc	oxygen	0.07±0.08	0.09	15	0.04±0.05	0.06	17	0.18±0.13	0.12	25	0.11±0.10	0.12	21	0.35±0.01	0.21	2	–	0.24	0

Table 18. MEAN AMPLITUDE RATIOS

Variability Type	Spectral Type	1.25/2.2 Δmag/Δmag	N	2.2/3.5 Δmag/Δmag	N	3.5/4.9 Δmag/Δmag	N	4.9/12 Δmag/Δmag	N	12/25 Δmag/Δmag	N
Mira	OH/IR	1.44±0.28	7	1.01±0.28	11	1.11±0.22	12	0.96±0.09	4	1.19±0.09	3
Mira	oxygen	1.44±0.44	32	1.08±0.28	39	1.20±0.27	35	0.83±0.15	4	1.18±0.03	2
Mira	carbon	2.76	1	0.88±0.25	6	1.16±0.20	7	1.06±0.42	8	1.14±0.06	2
Mira	S	1.66	1	0.99±0.01	2	1.37±0.36	2	–	0	–	0
SRa	oxygen	0.95±0.51	4	1.19±0.18	5	–	0	–	0	–	0
SRa	carbon	2.06±0.15	2	1.29	1	–	0	1.31	1	–	0
SRb	oxygen	1.42±0.21	6	0.81±0.19	10	1.47±0.35	5	–	0	–	0
SRb	carbon	2.28±0.80	3	1.14	1	0.97	1	–	0	–	0
SRb	S	–	0	0.70	1	–	0	–	0	–	0
Lb	oxygen	–	0	0.69±0.03	2	–	0	–	0	–	0
Lb	carbon	–	0	1.00	1	1.22±0.12	2	1.45	1	–	0